Cold Bottom Water Events Observed in the Hawaii Ocean Time-Series: Implications for Vertical Mixing

Roger Lukas

Fernando Santiago-Mandujano

Frederick Bingham

Arnold Mantyla

Submitted to Deep-Sea Research
Revised April 2000

ABSTRACT

During 1991- 1999 six near-bottom, cold-water anomaly events occurred at the Hawaii Ocean Time-series deep-ocean hydrographic station (22°45'N, 158°W), situated on the northern flank of a seafloor basin known as the Kauai Deep. Cold anomalies of at least 0.01°C, and as much as 0.024°C, were observed in near-bottom CTD profiles during each event. The anomalies relaxed towards more typical conditions over a period of several months. On the basis of water mass properties, we infer that the cold anomalies in the Kauai Deep originated when colder, saltier water from the adjacent Maui Deep spilled over the sill that separates these abyssal basins. The cause of these cold overflow events is not yet known, but inverted echo sounder observations and TOPEX/Poseidon altimeter data suggest that they might be associated with eddies entering the region of the Maui Deep.

The transport across the sill and the vertical structure of the eddy diffusivity parameter were estimated with a one-dimensional advection-diffusion model, considering the evolving shape of the anomalous potential temperature profile during the third event onset and the apparent overflow duration. The best subjective fit to the observations yields a transport across the sill of 0.18 Sv, and a constant vertical eddy diffusivity of 7×10^{-4} m^2 s^{-1}. The observations during the recovery of the anomalous temperatures for four of the events were used to calculate the terms of a one-dimensional diffusion model, yielding the vertical and temporal variability of the turbulent diffusivity. The results show a consistent picture of the eddy diffusivity reaching median values of 40×10^{-4} m^2 s^{-1} near the region of the sill depth and decreasing above and below it. This increase seems to be due to enhanced levels of turbulence near the depth of the controlling sill. The diffusivities also peak at the beginning of the relaxation period, decreasing by one order of magnitude at the end of each event.

The fifth event's overflow was apparently captured in progress with two full-depth CTD profiles obtained 46 hours apart, during which the near-bottom temperature decreased 0.035 °C, the salinity increased 0.003, and the dissolved oxygen increased 7 μmol kg^{-1}. A seiching motion or deep baroclinic basin mode resulting from the event could explain this and other large differences in near-bottom temperatures observed between deep casts taken a few days apart.

1 INTRODUCTION

Since October 1988, investigators at the University of Hawaii have been conducting a deep-ocean observational project, the Hawaii Ocean Time-series (HOT), funded by the National Science Foundation as part of the U.S. contributions to the World Ocean Circulation Experiment (WOCE) and the Joint Global Ocean Fluxes Study (JGOFS) programs (Karl and Lukas, 1996). The site for these deep-ocean observations is known as the HOT site, or Station ALOHA, located at 22°45'N, 158°W (Fig. 1a).

The details of the bathymetry deeper than 4400 m in the abyssal regions surrounding the HOT site according to the 5' ETOPO5 bathymetric dataset are shown in Fig. 1b. (The Smith and Sandwell [1997] seafloor topography product has higher resolution, but with spurious maxima and minima, so it is not used here.) The region to the north of Oahu is dominated by the Kauai Deep, which is between 4900 and 4950 m deep. The HOT site is in 4740 m of water on the northern flank of this basin. The Maui Deep is found to the southeast, with depths exceeding 5600 m. The controlling sill between these basins is about 100 km east of Station ALOHA in the Oahu Seamounts, between 4450 and 4500 m deep shown contoured in Fig. 1b. Another basin is located northwest of the Kauai Deep, reaching depths of 4850 m. The controlling sill between this basin and the Kauai Deep is approximately 4540 m deep and is located about 100 km west of Station ALOHA.

Anomalously cold near-bottom waters were observed at the HOT site during 1991, late 1993, late 1995, winter 1996-1997, late 1998, and late 1999 (Figs. 2 and 3). These cold events were of varying duration, but in each case the temperature profile relaxed towards normal over a

period of several months. Such transient events in the abyssal ocean have been observed previously by other investigators (cf. Schwartzlose and Isaacs, 1969; Whitehead, 1989; Johns et al., 1993), but with much coarser vertical resolution than the observations reported here.

The cold events that we have observed are consistent with a picture of the bottom water circulation that is sluggish in general, but subject to surges associated with event-like sloshing and overflow of bottom waters from one abyssal basin to the next. The dynamics responsible for these surges are unclear.

These cold surges have important implications for our conceptual model of abyssal vertical diffusion of heat, which is undergoing considerable revision (cf. Polzin et al., 1996, 1997). Analysis of the evolution of the cold events in the HOT observations allows us to estimate near-bottom vertical eddy diffusivity; the magnitudes derived are unexpectedly large. If such surges are the primary mechanism by which the bottom waters circulate, then the strong vertical mixing associated with these events may be an important contribution of vertical diffusivity of heat near the bottom.

In the rest of this paper, we first describe the cold events in detail (Section 2). Next, we discuss the abyssal Pacific Ocean circulation and previous observations of cold episodes in the bottom waters, as well as the possible dynamics of the cold events (Section 3). Estimates of the relative levels of mixing at different heights above the bottom, inferred from simple models that simulate the observed evolution of near-bottom temperatures, are presented in Section 4. Discussion of these results and some hypotheses about the causes of the cold events are found in Section 5, followed by a summary in Section 6.

2 OBSERVATIONS

Below, we describe various aspects of the cold events at the HOT site as observed by our repeated CTD profiling between October 1988 (cruise HOT-1), and November 1999 (cruise HOT-109). We focus on the temporal evolution of near-bottom temperature profiles, but also discuss the signatures of the cold events in salinity, dissolved oxygen and nutrients.

Occupations of the HOT site are approximately monthly. We obtain continuous profiles of temperature, salinity, density, and dissolved oxygen using a Sea-Bird conductivity-temperature-depth (CTD) profiler, which is calibrated frequently by the manufacturer, in our laboratory and against water samples collected during profiling operations. Dual sensor pairs have been used since June 1994 to detect problems that could corrupt the measurements, and to provide empirical estimates of the quality of the measurements. The accuracy and precision of our observations are given in Table 1. After processing, the vertical resolution of these profiles is about 2 m. Details concerning hydrographic data collection and processing are available in Lukas and Santiago-Mandujano (1996), and in the HOT program data reports (cf. Santiago-Mandujano et al., 1999). A comprehensive summary of observations made under the HOT project is provided by Karl and Lukas (1996), and Lukas and Karl (1999).

To attempt to understand the forcing mechanism(s) for the cold events, we used weather data obtained by the National Weather Service for sites around the Hawaiian Islands and an offshore buoy. We examined sea level data from tide gauges at harbors around Hawaii and we also make use of inverted echo sounder time series deployed near the HOT site (Chiswell, 1996), as well as TOPEX/Poseidon satellite altimetry (Mitchum, 1996).

2.1 Potential Temperature (θ)

Pronounced cold events occurred in mid-1991, late 1993, late 1995, during the winter of 1996-97, late 1998 and late 1999 (Fig. 2). Weak cold events seem to have occurred in early 1992 and in late 1994. There appears to be a tendency for cold events to occur during the winter, although the 1991 event occurred in late spring. This suggests a mechanism which is either part of the annual cycle, or which is modulated by it.

The first four cold events appear to be vertically coherent below the sill depth, and to about 50 m above the sill (e.g. event 4), but the coherence breaks down rapidly above that point (Fig. 2). The last two events were more intense and their signature extends up to 4200 m. However, the dominant variability between 4300 and 4500 m is the inter-annual variability studied by Lukas and Santiago-Mandujano (1996). Some of that signal clearly extends below the depth of the sill, and may influence the dynamics of the cold events.

Figure 3 shows the ensemble of potential temperature profiles below 4200 m for all deep CTD casts made during HOT cruises 1 through 109. (The maximum depth of each cast varies from cruise to cruise depending on such factors as length of wire on the winch, condition of the conducting cable, and weather.) An envelope of roughly ±0.005°C surrounds the ensemble median (heavy line in Fig. 3a) above 4400 m. This spread of temperatures is associated with inter-annual variations of the deep water (Lukas and Santiago-Mandujano, 1996), and high-frequency internal waves (Lukas and Santiago-Mandujano, 2000). Below 4400 m, the envelope widens from about ±0.01°C near 4500 m to ±0.015°C near the bottom.

The standard deviation increases from 0.005°C to 0.008°C within 100 m of the bottom, with

larger deviations towards colder temperatures, as indicated by the negative skewness. In many of the profiles, the vertical temperature gradient weakens noticeably below about 4500 m, so simple vertical displacements of the mean structure in the Kauai Deep cannot account for these signals. These cold extremes are associated with the 6 distinct events mentioned earlier, where colder waters appeared first at the deepest levels. It is interesting to note that the negative skewness only occurs below 4300 m reaching a maximum absolute value at the sill depth, and positive skewness occurs above 4300 m, suggesting that the sill depth is a boundary for two different physical regimes.

Over slightly less than the one month between cruises 25 and 26, potential temperature near 4600 m decreased from 1.107°C to 1.097°C (Fig. 4). The deep casts during the three previous cruises (22-24) were not deep enough to obtain data around 4600 m, or even to indicate when the cold event started to develop. During the two cruises after HOT-26, casts were made closer to the bottom allowing a determination of the magnitude of the cold event and its vertical distribution. Information relevant to this and the other cold events is included in Table 2. Cruise 27 had a minimum value of 1.086°C near 4700 m, 0.012°C colder than the median. This is a very large anomaly for the abyssal North Pacific. Over the next several cruises, the near-bottom water warmed (though not uniformly, note that cruise 29 is warmer than 30 and 31). This is a characteristic common among the cold events. It took about 200 days for the bottom waters to recover from the cold event. An exponential fit to the potential temperature averaged between 4590 and 4625 m yields an e-folding time scale of 123 days for the recovery (Fig. 4, Table 2).

The second cold event is apparent in the ensemble of potential temperature profiles from cruises 46-56 (Fig. 5a). Casts starting with cruise 49 have maximum depths closer to the bottom

(below 4700 m) than in previous cruises. The ensemble of profiles shows an envelope comparable to that observed in the first event.

Because our CTD casts were closer to the bottom, the onset of the second event was observed in more detail than during the first event. One common feature of the profiles during the recovery phase is that they exhibit negative curvature ($\partial^2\theta/\partial z^2 < 0$). An additional feature observed in some of these profiles is a near-constant potential temperature layer below ~4670 m, located beneath the abrupt gradient between 4600 and 4650 m. This feature was not observed during the first event, probably because the casts were not deep enough, but it is also seen in some of the casts during the recovery phase of the following four events. The recovery period for this cold event was about 220 days. The exponential fit to the casts during the recovery period for this and the following three events was done to the mean potential temperatures between 4680 and 4707 m (Figure 6, Table 2).

A third major cold event was observed during cruises 65 through 74. Potential temperature profiles during cruises 65 and 66 have a sharp thermocline below 4700 m, with near-bottom temperatures about 0.01°C colder than those above the interface (Fig. 5b). In sharp contrast to the cooling below, the mean potential temperature around (and above) 4700 m increased from cruise 64 by more than 0.005°C over the following two months (Fig. 6). The potential temperatures below 4700 m continued decreasing, reaching a minimum of 1.088°C at 4720 m during cruise 68. It is remarkable that the cooling from cruise 67 to 68 extended upward to about 4400 m, clearly suggesting an upward propagation of the event. The onset of this event lasted at least for the 110 days between HOT-64 and HOT-68. After cruise 68 the temperatures started to increase, reaching the warmest values about 250 days later during HOT-74.

A more intense cold event occurred between cruises 74 and 88. Potential temperatures started decreasing after HOT-74 (Fig 5c). All the casts during the cooling period exhibit a nearly 50 m thick constant temperature layer right above the bottom, located immediately below the region of strongest temperature gradient. This is in contrast to what was observed during the third cold event, where profiles during the cooling period exhibited a sharp thermocline very close to the bottom. Temperatures started to increase after cruise 78, but they remained relatively cold at 4700 m (0.007°C below the median) during cruises 80 through 85, and did not return to the pre-event conditions until HOT-88, nearly one year after the coldest temperatures were registered.

The most intense event observed during the study period occurred between cruises 98 and 106. During cruise 98 two full-depth profiles were obtained separated by 46 hours (Fig. 5d). The first profile shows near-bottom temperatures warmer than the median, while the second profile's temperatures are the coldest that have been observed, and they developed over a remarkably short time interval. In the lowest 50 m, the potential temperature decreased 0.035 °C between casts. At a height of about 100 m above the bottom, the changes were substantially less, being well within the normal range of variability. The temperatures started to increase after this cruise, with the cooling extending upward to about 4200 m during cruise 99. The temperatures returned to near normal conditions during cruise 106, about 265 days after the beginning of the event, just before a sixth event started, as indicated by the observations from cruise 107 (Fig. 5d). The cooling also extended upward to about 4200 m during this cruise. The temperatures started to increase after this cruise and had returned to near normal conditions by the end of the

observation period (November, 1999).[1]

2.2 Other Hydrographic Variables

Salinity below 4200 m during the cold events has an envelope of variability of roughly 0.003, comparable to the accuracy with which salinity can be determined using present state-of-the-art methods (Table 1). However, cruise-to-cruise consistency may be closer to 0.001 because we use a very stable substandard to bridge batches of IAPSO standard water and to make more frequent standardization readings on our salinometer. The deep salinity shows an increase of about 0.002 during the first event and the other events show an increase of about 0.002-0.003 with respect to cruises surrounding the cold events (e.g. Fig. 7a). The slope of the salinity vs. depth curves seems to change during the events onsets, exhibiting positive curvature ($\partial^2 S/\partial z^2 > 0$). For example, the profile from cruise 78 has a 0.003 increase in salinity between 4300 m and the bottom, coinciding with the decrease in temperature observed over the same depths during the fourth event (Fig. 5c).

Our CTD dissolved oxygen profiles are somewhat noisy, and their accuracy (Table 1) depends strongly on the quality and distribution of discrete water samples used for calibration. The discrete sampling for dissolved oxygen concentration is too sparse for a proper description of dissolved oxygen variation associated with the cold events, but the available data show an increase of about 2-3 μmol kg^{-1} relative to the cruises surrounding the cold events. This is larger than the precision of our Winkler titrations (roughly 0.15%; Winn et al., 1993) but is comparable

[1] A preliminary analysis of data obtained after November, 1999 indicate that conditions were back to normal by April 2000, about 230 days after the beginning of the event.

to the accuracy of the method. Smoothed CTD oxygen profiles during the fourth event show this increase (Fig. 7b). As in the case of salinity, these profiles also show a positive curvature ($\partial^2 O_2/\partial z^2 > 0$) during the onset of the events.

The extreme temperatures observed in the development of the fifth event during cruise 98 are also reflected in the salinity and oxygen concentrations. In the lowest 50 m, the salinity increased 0.003, and the dissolved oxygen increased 7 μmol kg^{-1} between the first and the second deep casts (Fig. 8).

Our measurements of inorganic nutrients (nitrate+nitrite, soluble reactive phosphorus (SRP), and silicate) obtained from water samples provide limited information about variations that might be associated with the cold events. The envelope of variability in the deep water is comparable to the range of uncertainty of the measurements. Also, the vertical resolution is insufficient to show any depth-dependent variability close to the bottom, as we follow WOCE standards and collect samples at 200 dbar intervals in the deep ocean. We do have a sequence of values from the deepest bottle of each deep cast. Deep values of nitrate+nitrite during the third and fourth cold events showed a decrease of about 0.8 μmol kg^{-1} compared to data from cruises before and after the events. However this variability is close to the 0.44 μmol kg^{-1} analytical uncertainty estimated from bottom water control samples from cruises 70-75. The measurements of SRP and silicate did not show a clear pattern of variability related to the events.

3 NATURE OF THE COLD EVENTS

How are the cold events observed by the HOT program related to the large-scale circulation

of abyssal waters? What are the dynamics associated with these episodes? What are the local impacts of these events? With the observations available to us, we cannot answer these questions. However, we develop some hypotheses below, which may be useful in guiding future observations.

3.1 Pacific Bottom Water Circulation

Mantyla (1975) and Mantyla and Reid (1983) describe the circulation of bottom water in the Pacific Ocean. The densest bottom water in the North Pacific flows across the equator in the central Pacific, fed by the northward flow in the Samoan Passage (Reid, 1969; Reid and Lonsdale, 1974; Roemmich et al., 1996). Edmond et al. (1971) show that Pacific Bottom Water penetrates to the east towards Hawaii through two narrow gaps in the Line Islands Ridge, the Horizon passage and the Clarion passage (Fig. 1a), with the flow through the Clarion passage being much weaker. Further, they infer that the flow occurs in the lowest 400 m. Figure 1a shows a possible bottom water path through the Horizon passage into the northeast Pacific (from their Fig. 9), and Fig. 9 shows the bottom topography along this path. Based on the available data, these authors argue that the Bottom Water dissipates east of Hawaii and that it is not detectable east of 152°W or north of 23°N. Near the Hawaiian Islands, there are potentially significant near-bottom horizontal temperature gradients due to this dissipation.

Cold bottom water penetrates eastward south of Hawaii, and recurves to the northwest along the north side of the Hawaiian Ridge as illustrated in Fig. 1a (Chung et al., 1969; Mantyla, 1975). Near-bottom potential temperature is more than 0.1°C warmer north of Oahu than northeast of the island of Hawaii, a separation of about 450 km. At 4500 m, Chung et al. (1969) show *in situ*

temperature increasing from 1.43°C east of Hawaii Island to 1.50°C north of Oahu. The observed temperature gradient along the north side of the Hawaiian Ridge was about 2.22 x 10^{-6} °C m^{-1}. A cold anomaly of 5 x 10^{-3} °C could be caused in about one day by a transient flow of 0.025 m s^{-1} towards the northwest. However, this gradient could be a transient feature itself, and may be subject to inter-annual variability in the deep waters such as seen by Lukas and Santiago-Mandujano (1996).

We hypothesize that the cold events described in Section 2 are due to flow of near-bottom water from the Maui Deep to the Kauai Deep (Fig. 9), over the controlling sill that separates these two basins, along the path illustrated in Fig. 1b. The near-bottom waters to the west of the Kauai Deep are warmer and fresher than at the HOT site (Mantyla and Reid, 1983), and thus could not have contributed to the cooling and salinity increase of the Kauai Deep bottom waters. Bottom water in the Maui Deep is sufficiently colder and saltier than at the HOT site such that overflow from the Maui Deep could easily have caused the changes seen during the onset of the cold events described in Section 2. CTD profiles obtained on 27 April 1998 from the western slope of the Maui Deep (22.22°N, 156.61°W), and from the sill site (22.62°N, 156.96°W; Fig. 1b) are shown in Fig. 10 together with a deep profile from HOT-92 conducted one week earlier. No cold event was occurring during this cruise so this profile is representative of "normal" conditions at ALOHA. The near-bottom water from the Maui Deep was about 0.023°C colder and 0.003 saltier than the near-bottom water at Station ALOHA at comparable depths. (There were no oxygen bottle data available to calibrate the Maui Deep CTD oxygen profile, so we cannot make a useful comparison between the sites.) Salinity differences between the two basins on potential density surfaces are much smaller (Fig. 10c) than the magnitude observed during strong cold events. To account for the temperature and salinity anomalies observed during the

fourth cold episode, waters of σ_5=50.240 from the Maui Deep must have displaced waters of σ_5=50.234 on the sill. In order to account for the temperature and salinity anomalies in the Kauai Deep during event 4, water in the Maui Deep must have been displaced from near 4800 m upward by at least 300 m to clear the sill. This is a substantial displacement, and one wonders what forcing produces that displacement. This is discussed in Section 3.3.

Surges of cold bottom water similar to those described here have also been observed in the western North Atlantic (Whitehead, 1989), in the western tropical Atlantic (Johns et al., 1993), and in the eastern equatorial Atlantic (Polzin et al., 1996).

3.2. Response of the Kauai Deep to cold overflows

While the HOT CTD profiles have captured these six bottom water events, we do not have observations that fully resolve the temporal variability and we have almost no horizontal spatial information. During more recent cruises, we have made additional full-depth CTD profiles when time has permitted, and these allow us to comment on short-term temporal variations (e.g. the development of the fifth event during cruise 98), and small-scale spatial variations (cf. Appendix in Lukas and Santiago-Mandujano, 1996).

During the cold overflow, internal gravity wave energy would almost certainly be enhanced as the cold water equilibrates in the depths of the Kauai Deep. Depending on the volume transport of the overflow, it is possible that a seiching motion could result that would slowly damp out as energy was carried away by internal gravity waves and by dissipation in the benthic boundary layer. Such a seiching motion might explain the large differences in near-bottom

temperature between two CTD profiles during HOT-58 (Lukas and Santiago-Mandujano, 1996), and the extremely fast near-bottom cooling between two CTD profiles during the fifth event. It is possible that the observed anomalous bottom water was present in the Kauai Deep during the first cast of HOT-98 (from a prior cold overflow event), but not observed in that profile because of some type of deep-basin seiching. (This is explored further in section 3.3). The enhancement of internal gravity wave energy would likely result in an increased frequency of overturns and turbulent mixing. Because of the shape of the basin and the distribution of bottom slopes, there might be focal points at various locations and heights above the bottom for internal wave packets of various frequencies to converge, creating a complex vertical and horizontal distribution of turbulent kinetic energy. In any case, it is reasonable to expect that turbulent kinetic energy levels will increase near the bottom during and after cold overflows. This is explored further in Section 4.

3.2.1. Transport and upwelling estimates during cold events

The ETOPO5 bathymetry data (nominal 5 nm horizontal resolution) was used to compute the area, $A(z)$, enclosed by specified isobaths in the Kauai Deep and the volume, $V(z)$, of the basin as a function of depth (z) (Fig. 11). We estimate the basin-wide-average upwelling speed, $w(z) = Tr/A(z)$, for a given volume transport (Tr) over the sill by assuming that bottom waters of the Kauai Deep are replaced from its deepest point by water overflowing from the Maui Deep (as illustrated in Fig. 9b). This implicitly requires that the colder, heavier water flows from the sill to the bottom of the Kauai Deep without mixing which might be reasonable for small overflow rates. Figure 11 shows the upwelling profile for an arbitrary transport of 0.05 Sv. The duration of the overflow (V/Tr) needed to reach a specified level is calculated by assuming a constant

overflow rate. Fig. 11 suggests that a transport of 0.05 Sv would cause the anomalously cold water to penetrate upwards from the bottom of station ALOHA to 4650 m in about 200 days. This is roughly the level reached by the cold water during the onset phase of cold events as suggested by the CTD profiles (Fig. 5). The mean upwelling speed in this depth range is about 0.5 m d^{-1}. These estimates of transport and upwelling are too low if the overflow event was shorter than 200 days in duration (as in the case of the third, fifth and sixth events), and too high if the shallowest level reached by the cold water was below 4650 m.

The fifth cold event had a particularly rapid development during cruise 98, penetrating at least 50 m upwards from the bottom of station ALOHA during the 46 hour interval between deep casts (Fig. 5d). According to Fig. 11, with a constant transport of 0.05 Sv it would take about 100 days for the cold water to upwell 50 m from the bottom of station ALOHA. This implies that the transport across the sill would have to have been about 2.5 Sv for the colder water to upwell this far in only two days. This unreasonably large value suggests that an additional mechanism, such as the deep-basin seiching mentioned in the last section, must have been associated with the rapid cooling observed during this cruise. For a single node seiche model (Fig. 12), the first deep cast of the cruise would have been taken when the warm water was displaced downwards at the HOT site, while the second deep cast would have been made when the cold water from the cold event was displaced upwards.

3.2.2. Heat content estimates

Heat content in the Kauai Deep basin was calculated from the bathymetry data and the CTD potential temperatures profiles at ALOHA. Assuming that θ is horizontally homogeneous throughout the basin, the heat content per unit depth is

$$q(z,t) \approx \rho C_p A(z)\theta(z,t) \qquad (1)$$

where *A(z)* is the area of the Kauai basin calculated from bathymetry data, and $\theta(z,t)$ is from the station ALOHA CTD profiles, C_p is the specific heat capacity at constant pressure (~ 4 X 10^3 J $kg^{-1}°C^{-1}$) and ρ is density. The total heat content of the Kauai Deep was obtained by integrating from the deepest point at station ALOHA (z_0) to the depth of the sill (z_s) that separates this basin from the Maui Deep,

$$Q(t) = \rho C_p \int_{z_0}^{z_s} A(z)\theta(z,t)dz \qquad (2)$$

The CTD profiles during the first event are too shallow to provide an adequate estimate of the heat content, and were not used. This integral was evaluated by trapezoidal approximation for the period including events two through six, from 4685 m (the deepest common level of the profiles) to 4488 m (sill depth) (Fig. 13). During the second and fourth events the coolest temperatures appear after a long period (4 to 7 months) of decrease in the heat content, while during the third, fifth and sixth events this decrease coincide with the decrease in the temperature. Maximum heat content losses occur during the fourth, fifth and sixth events. A period of heat gain follows after the coolest temperatures appear near the bottom during each event.

3.3 Dynamics of cold overflow events

What forced the overflow of abyssal waters from the Maui Deep into the Kauai Deep? There is no obvious periodicity for these events though, as mentioned in Section 2, there seems to be a

tendency for the cold events to occur during the winter months (Fig. 2). A much longer time series would be required to determine a statistically significant linkage with the annual cycle. In any case, it seems that the forcing mechanism(s) must be intermittent. Some events occur very rapidly, on the order of days. Other events seem to develop over an interval of several months.

We consider the following candidate forcing mechanisms: 1) local winds, 2) rapid atmospheric pressure changes, 3) mesoscale eddies, 4) Rossby waves and 5) variable barotropic boundary currents along the northern flank of the Hawaiian Islands. The first two mechanisms would be related to relatively high frequency barotropic processes while the latter two are more likely to be low-frequency and baroclinic in nature. With only six observed events, there is no possibility of statistical analysis to reveal forcing physics. The following section is presented with the idea of developing useful working hypotheses to guide future observations.

Time series of wind and sea level pressure (SLP) from National Weather Service airport stations in the Hawaiian Islands (not shown), have been inspected for the periods surrounding the first four cold events. The onset of the first event does not seem to be related to any storm system, although it was preceded by a small drop in SLP and a modest increase in wind. The time of this event in late spring is when trade winds are fairly steady and neither cold fronts nor tropical storms influence the islands. The onset of the second event occurred during the passage of a cold front, where SLP returned to normal levels after a sharp drop, and winds strengthened considerably over the northern islands (Kauai, Oahu, Maui). The timing of the third event, in the fall, does not seem to be related to any tropical or extratropical weather system, although it did occur during a period of energetic high frequency wind fluctuations. The fourth cold event was first observed right after a strong high-pressure cell (in the wake of a cold front to the north of

the islands) increased the trade winds sharply, especially at Lihue, on Kauai.

A barotropic response to local weather forcing might be expected to have an observable sea level signal in the tide gauges maintained at harbors in the Hawaiian Islands. These records (not shown) have been inspected carefully during the first four events. Each event onset is preceded by an increase in sea level, which is consistent with a drop in SLP. However, there are many more pronounced increases in sea level that do not correspond to a cold event, and no conclusion can be drawn from the island sea level records.

Inverted echo sounder (IES) records at and near the HOT site (Chiswell, 1996), might reveal baroclinic signals that are related to the forcing of the cold events, however there are no IES data available during the last two events. In the IES record and in TOPEX/Poseidon altimeter data there is energetic variability at periods of about 130 days (Chiswell, 1996; Mitchum, 1996), which propagates westward. This appears to be related to baroclinic Rossby waves, but with more complex vertical structure rather than the first baroclinic mode. The first four events considered in the present study occurred during or just after a relative minimum of dynamic height (Fig. 14). During the second and fourth events, the near-bottom temperatures started to decrease during a period of decreasing TOPEX/Poseidon height, during a relative minimum for the third event, and during a rapid drop in the TOPEX/Poseidon height for the fifth event, possibly indicative of the passage of a cyclonic eddy or a Rossby Wave trough. Such eddies may have significant near-bottom currents even though the strongest current fluctuations are in the upper water column. However, other drops in the TOPEX/Poseidon height record are not associated with any cooling of the bottom water. Thus, the only conclusion that might be drawn is that a low sea level signal may be a part of the dynamics of the cold events, but that it is not

sufficient to cause an event.

An alternative mechanism for the generation of a seiching motion in the Kauai Deep would be the deep velocity signature of a passing eddy. Given that the typical Rossby radius at the HOT site for the first baroclinic mode is 45 km, which is approximately the radius of the Kauai Deep, a passing eddy might resonantly excite a deep baroclinic basin mode. Such a mode might be a standing wave, or possibly a progressive wave composed of one or more Kelvin waves. These baroclinic modes such as a Kelvin wave might be excited also in the Maui Basin, and could lead to overflows at the sill by lifting the isopycnals at the edges of the basin.

The interannual variability extracted from the TOPEX/Poseidon altimeter data near the HOT site (Fig. 15) also shows a signal that might be related to the cold events forcing. This signal reveals a pattern of westward propagation that was not obvious in the previous analysis of a shorter time series by Mitchum (1996). The westward speed of the relative minimum observed between 1993 and 1995 is about 0.08 m s^{-1}. This interannual variability at the HOT site seems to be related to biennial fluctuations of the Deep Water described by Lukas and Santiago-Mandujano (1996). These fluctuations have been associated with vertical displacements of the mean thermal structure by baroclinic Rossby waves, possibly forced by remote low frequency fluctuations in the surface wind field. During events two through five when TOPEX/Poseidon data are available (Fig. 15), the temperatures started to decrease during (second and fourth events), or after a drop in the TOPEX/Poseidon height (third and fifth events).

The time series of barotropic meridional transport along the northern coast of the Hawaiian Islands calculated from monthly FSU wind data between 1988 and 1999 and assuming that boundary flows close the Sverdrup flow under a time-varying “island rule” (Firing et al., 1999),

also show signals that might be related to the cold events (Fig. 14). During the third, fourth and fifth events, and even during the weak cold events described in Section 2 (early 1992 and late 1994), the bottom temperatures started to decrease after or during a northward increase in the meridional transport, which may have induced the overflow of cold water from the Maui Deep to the Kauai Deep. However during the second event the temperatures showed a different pattern and started to decrease during an increase in the southern transport, and continued decreasing after the transport switched northward. During the first event the temperatures started to decrease during a northward increase in the transport, however the fastest temperature decrease occurred when the northern transport was decreasing. During the sixth event the temperatures started to decrease when the transport was near zero. The intense episode of northward transport increase in early 1995 does not seem to have triggered any cold event. The increase in the barotropic meridional transport during the winter months is associated with an apparent annual variability attributed to the wintertime intensification of the Subtropical High, and the latitudinal migration of the trade winds over the eastern North Pacific (Firing et al., 1999).

4 OVERFLOW AND RECOVERY MODELS: DESCRIPTION AND RESULTS

To estimate near-bottom vertical diffusivity and vertical velocity changes associated with the cold overflows, two simple models are used to exploit the observations of the cold anomalies. The first model assumes that the cold bottom water anomaly at the HOT site was due to an introduction of colder bottom water into the Kauai Deep surrounding station ALOHA, as described in Section 3, which is then upwelled. The upwelling cold water, together with possible changes to the downward (turbulent) diffusion of heat, alters the one-dimensional heat budget of

the Kauai Deep below the sill during the introduction of colder water into the basin. We call this the overflowing phase, assuming that during this time water overflows from the Maui Deep into the Kauai Deep through the shallower connecting channel.

Ignoring horizontal advection, and assuming that there are no horizontal temperature gradients within the Kauai Deep, the evolution of potential temperature during the overflowing period can be described by

$$\frac{\partial \theta}{\partial t} = -w\frac{\partial \theta}{\partial z} + \frac{\partial}{\partial z}\left(K_v \frac{\partial \theta}{\partial z} \right) \qquad (3)$$

where w is the vertical velocity and K_v is a general eddy diffusivity, which may vary with depth and time. For steady-state conditions, this is the simple balance between vertical advection and vertical diffusion that holds for the large-scale ocean circulation (Munk, 1966).

When the overflow of cold water into the Kauai Deep terminates, a recovery or relaxation phase of 150-250 days starts during which the bottom water warms up as described in section 3. During this phase one might assume that w=0 below the rim of the Kauai Deep except for high frequency internal gravity waves. Thus the relaxation of the potential temperature profile back to pre-event conditions can be ascribed to vertical diffusion of heat, and we obtain the simple equation,

$$\frac{\partial \theta}{\partial t} = \frac{\partial}{\partial z}\left(K_v \frac{\partial \theta}{\partial z} \right) \qquad (4),$$

governing the evolution of the temperature field in the Kauai Deep during the recovery period. We note that these simple models cannot handle complex events such as event #4, where

recovery from one overflow episode is not complete before another event starts. Such complex events must be relatively rare, since a continuum of events would result in a Gaussian distribution of temperature variability. The large negative skewness (Fig. 3) argues against that.

4.1. Boundary and initial conditions

The boundary and initial conditions for solution of Equations (3) and (4) are as follows. The bottom of the model ocean is insulated. That is, a condition of zero vertical flux of heat at the bottom or zero vertical temperature gradient at the bottom is assumed.

$$K_v \frac{\partial \theta}{\partial z} = 0, \quad \text{at} \quad z = H \tag{5}$$

where H is at the bottom. For modeling both phases of the cold events (overflow and relaxation) the temperature was assumed constant at 4300 m, above the sill depth, where the observed temperature variance is small (Fig. 3). For the overflow model the cold temperature near the bottom was kept constant to simulate a continuous input of cold water at the bottom of the basin (see below).

The relaxation problem is equivalent to the determination of the temperature distribution in a solid bar which is held at a constant temperature at one end and insulated at the other and whose thermal conductivity may vary. A small flux of heat has been observed from the seafloor to the deep ocean (Lee and Cox, 1966) which can affect the bottom waters (Joyce et al., 1986), so one model run was done with a constant geothermal heat flux into the bottom of the water column to estimate the possible magnitude relative to the recovery from cold events.

A smoothed version of a temperature profile from station ALOHA between 4180 m and the bottom was used as an initial condition. The overflowing phase was modeled based on profiles obtained during the third event. This event was selected because it does not seem to be associated with a deep-basin seiche motion (such as that suggested for the fifth event), whose mechanism is not included in our simple model from Equation (3). The third event apparently started shortly after the HOT-64 cruise, when the temperatures between 1000 and 4400 m were anomalously high compared to previous cruises. Rather than using this anomalous profile as an initial condition, we used the HOT-65 temperatures in the 4180-4660 m range to specify the initial conditions for the model. This profile was smoothed with a 10 m Gaussian filter. Since the deepest bottom depth of the Kauai Deep is 4930 m, much deeper than at station ALOHA, the near-constant temperatures at 4660 m from the HOT-65 profile were extrapolated to 4880 m, and smoothly reduced to 1.085°C between 4880 and 4920 m to resemble the input of cold water near the bottom of the basin.

The recovery phase was also modeled based on profiles obtained during the third cold event. The smoothed temperature profile for HOT-68 (the beginning of the recovery) was used as an initial condition.

4.2. Model Solutions

4.2.1. Model of the Overflow

Equation (3) was solved using a Lax-Wendroff scheme for the advective part, with averaged central differences for w, and a forward time centered space scheme for the diffusive part (Press

et al., 1992). The vertically-variable velocity, *w(z)*, was calculated from the bathymetry data as described in section 3.2.1, assuming a constant transport, *Tr*, of water into the basin between overflow onset and termination. The main factors determining the model results (besides the initial condition profile) are *Tr*, and the eddy diffusivity K_v. *Tr* determines the upwelling speed of the cold water, while K_v determines the shape and curvature of the temperature profiles. The model run that (subjectively) best reproduced the magnitude and shape of the observed temperature profiles, as well as the duration of the overflow used a transport of 0.18 Sv and a constant eddy diffusivity of 7 x 10^{-4} m^2s^{-1}. Fig. 16 shows those results between 4300 and 4740 m (the bottom depth at station ALOHA). The initial condition is the curve farthest right in the figure, and the following curves are temperature distributions at 10-day intervals after the initial time. The curve furthest left (coldest temperatures) is after 110 days. The model adequately reproduced the decreasing temperatures observed during the 110-day overflow period between cruises 64 and 68 (Fig. 5b).

4.2.2. Model of the Relaxation

In order to obtain an objective estimate of K_v from the observations, equation (4) was integrated

$$\int_H^z \frac{\partial \theta}{\partial t} dz = K_v \frac{\partial \theta}{\partial z} + F_H(t) \qquad (6),$$

where $F_H(t) = -K_v \left.\frac{\partial \theta}{\partial z}\right|_{z=H} = 0$ (Eq. 5), and the terms involving θ were calculated from the data during the relaxation phase of the events to estimate values for K_v. An adequate evaluation of the

time derivative required a smooth estimate of the temperature relaxation to eliminate time variability not included in the model but apparent in the data (Section 2.1). A least-squares exponential fit similar to that described in Section 2.1 (Fig. 4) was applied to the potential temperatures averaged at 20 m intervals between 4000 m and the bottom, and the resulting temperatures were used to calculate the vertical derivatives using a cubic spline fit. A trapezoidal approximation was used to calculate the vertical integral of the time derivatives of the exponential fits. These calculations were applied to the potential temperatures during the relaxation phase of the 2nd, 3rd, 5th, and 6th events; the large time variability of the temperatures during the 1st and 4th events did not allow an adequate evaluation of K_v.

The vertical distribution of the median values of K_v during the 2nd, 3rd, 5th, and 6th events relaxation phase (Fig. 17a) shows peak values averaging almost 40 x 10^{-4} m^2 s^{-1} in the region near the sill depth, decreasing to about half the maximum value at 4000 m, and decreasing one order of magnitude near the bottom. The time variability of K_v is similar for each of the events and is illustrated by the results from the second event (Fig. 17b). Values of K_v peak at the beginning of the relaxation period, decreasing one order of magnitude by the end.

An alternative numerical simulation approach also confirmed increasing values of K_v near the sill depth during the relaxation phase of the third cold event. Equation (4) was solved using an implicit finite-difference scheme, and the boundary and initial conditions specified in Section 4.1. The resulting temperatures were subjectively compared against the observed relaxation profiles from the third event. The run that best reproduced the duration of the relaxation as well as the curvature of the profiles (not shown) was with a vertically-variable diffusivity of 18 x 10^{-4} m^2 s^{-1} between 4300 and 4600 m, and of 8 x 10^{-4} $m^2 s^{-1}$ below 4600 m. If Equation (4) describes

the primary heat balance for the recovery of the deep water events, a simple scaling of the equation using values derived from Fig. 6 shows the diffusivity to be the right order of magnitude.

In order to determine if geothermal heating was potentially important in the recovery from the cold event, a model run was performed using a constant heat flux bottom boundary condition. A value of 59 mW m^{-2} was used for the geothermal heat flux; this value is considered 'typical' of the region near the HOT site (M. Mottl, personal communication). At the end of 200 days, the temperature difference between this model run and the one without bottom heating was about 0.002°C, which is a factor of five smaller than the total warming observed. We thus conclude that geothermal heating was not a significant factor in the warming of the bottom water, unless anomalous geothermal activity was occurring. The Kauai Deep is far from known geothermally active areas.

5 DISCUSSION AND CONCLUSIONS

The roughly 200 days required for near-bottom temperatures at station ALOHA to recover from the cold overflow events suggests a relatively large vertical diffusivity. The e-folding time scale for the recovery phase of the events varied between 70 and 190 days. This in turn suggests that processes which create turbulence near the bottom of the ocean may be episodically energetic (cf. Schwartzlose and Isaacs, 1969), and that a concerted observational effort would be needed to properly measure the mean diffusivity.

The diffusivities obtained from the models above may seem rather large compared to earlier

values estimated for the deep ocean (Munk, 1966, Toole et al., 1994). Increasing evidence has revealed that abyssal circulation over sills and through constrictions is often associated with high levels of mixing. Polzin et al., (1996) measured intense levels of mixing in the Antarctic Bottom Water flowing to the eastern equatorial Atlantic along narrow passages and over sills, suggesting strong near-bottom vertical shears and hydraulically-controlled flows as possible sources of turbulence. Other observations in the Atlantic (Polzin et al., 1997; Ferron et al., 1998), Pacific (Roemmich et al., 1996), and Indian Oceans (McCarthy et al., 1997), confirm that high levels of mixing (one to three orders of magnitude larger than rates measured in the ocean interior) are associated with bottom water flows constricted by sills and abyssal passages.

An important question is raised by this set of observations: What fraction of replenishment of bottom waters in the Kauai Deep is associated with such events, versus a more continuous process of replenishment that has been envisioned as part of the traditional model of bottom water circulation?

In the Deep Western Boundary Current of the North Atlantic, surges of cold bottom water appear to be fairly regular, exhibiting a tendency for a 60-70 day periodicity (Johns et al., 1993). The causal mechanism for these surges was not determined, however it was suggested that eddies associated with surface current instability with this preferred periodicity might have a significant barotropic component (Johns et al., 1990). It is also possible that the surges may be forced by overflows from basins further upstream with respect to the bottom water circulation. For example, Whitehead (1989) observed surges in the Demerara Abyssal Plain, which occurred with a 60-day periodicity.

What is the cause of the cold events observed at Station ALOHA? We have established that

the anomalously cold water originates in the Maui Deep, and infer that it episodically pours over the sill that separates the two abyssal basins. Limited observations suggest that colder, saltier waters from the Maui Deep may have to be displaced upwards by as much 300 m in order to explain the observed anomalies. Flow towards the west-northwest in the Maui Deep is required to cause sufficient convergence and upwelling near the sill. Such flow may be forced by local weather events, or remotely forced.

Some overflow events have a very rapid onset and relatively short duration, while others appear to be sustained over several months. It may be that several forcing mechanisms exist, and there may never be a clear correlation between any one mechanism and the occurrence of the cold overflows. Further, there are likely to be threshold effects introduced by the topography. The overflow from the Maui Deep reduces the volume of cold water available to the overflow. Another way to view the situation is that after an event, the potential thermal anomaly for a given "slosh" amplitude is reduced. To achieve the same potential requires replenishment of the Maui Deep bottom waters; that replenishment may be episodic as well. Another threshold effect is due to the position of the HOT site along the flank of the Kauai Deep. Cold overflows which have a total volume less than that of the Kauai Deep below the depth of the HOT site will not be directly observed there, and the upwardly diffused signal may be difficult to detect.

Barotropic pressure changes may be associated with rapid sea level pressure changes, such as when a cold front passes. These frontal passages are very short-lived, and would be expected to generate very short duration overflows. The strong surface wind stress associated with frontal passages may excite near-bottom flows through the generation of barotropic Rossby waves. Even though these waves travel very rapidly, their length scale can be very large, and they may give

rise to more sustained events even though the forcing is associated with high frequency weather. Because of the threshold effects mentioned above, it is clear that not every large amplitude weather event will result in a cold overflow that is detectable at Station ALOHA.

Low frequency barotropic adjustment to changing wind stress curl between Hawaii and North America may cause sufficiently strong and rapid boundary currents along the northern flank of the Hawaiian Ridge that they may cause some of the observed cold events.

Alternatively, a barotropic Kelvin wave excited in the Maui Deep by some forcing mechanism could lift isopycnals at the edges of the basin and cause an overflow through a gap at the sill.

Other forcing mechanisms that may give rise to flows in the Maui Deep leading to cold overflows include mesoscale eddies and long baroclinic Rossby waves. Even for a flat bottom ocean, standing baroclinic modes have a non-zero horizontal velocity signature at the bottom. When encountering topographic features like these abyssal basins and the sill that separates them, the horizontal and vertical velocities are likely to be amplified. Lukas and Santiago-Mandujano (1996) observed interannual near-bottom temperature signals at Station ALOHA, suggesting their connection to ENSO events and remote forcing. A mix of interannual and annual Rossby waves might explain the tendency for the overflows to occur in the winter half of the year, but not every year. The flows associated with these slower waves may not cause the overflow itself, but may be important to establishing the thermal anomaly potential for any given impulsive event.

The observations reported here have allowed us to estimate the heat budget, as well as the

vertical diffusion of heat by turbulent processes near the bottom north of Hawaii. A significant amount of heat (about 10^{17} J) is redistributed within the Kauai Deep during the cold events. If the surges of bottom water that occur in other locations are also associated with elevated levels of turbulent diffusion, it would contribute to the reconciliation between Munk's (1966) canonical value of vertical eddy diffusivity of 1×10^{-4} m^2s^{-1} and the accumulated evidence which suggests that actual values are one to several orders of magnitude larger (Toole et. al., 1994, Polzin et al., 1996, 1997; Ferron et al., 1998; Roemmich et al., 1996; McCarthy et al., 1997).

6 SUMMARY

The near-bottom, cold-water anomaly events observed in the Hawaii Ocean Time-series station are consistent with a description of cold water spilling from one deep basin into another. Increased levels of turbulence that redistribute vertically the heat near the bottom apparently accompany this process.

To clarify the dynamics of the cold events requires further research. With observation of only six events, we have no hope of extracting such information statistically, even if we had more spatial information and observations of other variables such as currents. It does seem clear, based on water mass analysis, that the cold, and salty anomalies observed in the Kauai Deep are due to flow of more denser waters from the Maui Deep over the sill separating the two abyssal basins.

To guide further observations which are required if the dynamics are to be understood, we propose the following working hypothesis. The Maui Deep is a reservoir of cold, relatively salty, Pacific Bottom Water. In analogy to the discharge of a capacitor, for a particular isopycnal, there

is some threshold level relative to the depth of the sill, below which overflow (discharge) is not possible given the typical spectrum of forcings. When the isopycnal is above the critical level, one or more of the potential forcing mechanisms listed in Section 3.5 *may* trigger an overflow. Thus, there may be different causes among the events and even multiple causes of a single event. The return interval of such an event-like phenomenon is the primary statistic of what is an exponential (Poisson) process.

The interval between events is governed by the recharge rate, the overflow volume, and the complex (magnitude and phase) spectrum of forcings. To the extent that the recharge of the Maui Deep is itself an event-like process, the distribution of Maui-to-Kauai Deep overflows is nonstationary. Likewise, the forcing spectrum is very possibly nonstationary. Thus, even with observation of many events, the statistical approach is unlikely to be successful in testing the hypothesis developed above. Rather, a deliberate numerical modeling approach, with *in situ* verification, is indicated.

We have modeled the impact of the cold overflows on the vertical distribution of heat in the Kauai Deep, extracting some information about vertical mixing in the process. The results show peak vertical eddy diffusivities of about 40×10^{-4} $m^2 s^{-1}$ in the region near the sill depth at the beginning of the relaxation phase of the events, decreasing above and below this depth, and decreasing one order of magnitude with time. These results indicate the importance of the vertical and temporal variation of the turbulent diffusivity of heat in the Kauai Deep associated with cold overflow events.

ACKNOWLEDGMENTS

We gratefully acknowledge the contributions of the scientists, technicians, students and ship's crews who worked hard to obtain the high quality observations of the Hawaii Ocean Time-series. We especially recognize the perseverance of those individuals that made winches, wire, and CTD equipment work to obtain the deep ocean data reported here. Jefrey Snyder was particularly instrumental in this regard. Sharon DeCarlo provided expert assistance with the data processing, data management, and analysis. The continued outstanding support from Nordeen Larson, Ken Lawson, and the staff of Sea-Bird Electronics Inc. has been essential in maintaining and even improving the high quality of the CTD data. We thank Gary Mitchum for providing TOPEX data, and we thank Bo Qiu and Weifeng Miao for providing the output from their model calculations. Discussions with Bo Qiu and Gary Mitchum are gratefully acknowledged. Comments and suggestions from two anonymous reviewers greatly enhanced the presentation of this paper. The National Science Foundation supported this work under grants OCE-9811921 (RL, FS-M), and OCE-9303094. Observations were also obtained under grant OCE-8717195.

REFERENCES

Chiswell, S.M., 1996: Intra-annual oscillations at Station ALOHA, north of Oahu, Hawaii. Deep Sea Res. II. Vol. 43, 305-319.

Chung, Y., M.L. Bell, J.G. Sclater, and C. Corry, 1969: Temperature data from the Pacific Abyssal Water. SIO Reference 69-17. Scripps Institution of Oceanography, Univ. Calif. San Diego, 75 pp.

Edmond, J.M., Y. Chung, and J.G. Sclater, 1971: Pacific Bottom Water: Penetration east around Hawaii. J. Geophys. Res., 76, 8089-8097.

Ferron, B., H. Mercier, and K. Speer, 1998: Mixing in the Romanche fracture zone. J. Phys. Oceanogr., 1929-1945.

Firing, E., B. Qiu, and W. Miao, 1999: Time-Dependent Island Rule and Its Application to the Time-Varying North Hawaiian Ridge Current. J. Phys. Oceanogr., 2671-2688.

Johns, W.E., T.N. Lee, F.A. Schott, R.J. Zantopp and R. Evans, 1990: The North Brazil Current retroflection: Seasonal structure and eddy variability. J. Geophys. Res., 95, 22,103-22,120.

Johns, W.E., D.M. Fratantoni, and R.J. Zantopp, 1993: Deep western boundary current variability off northeastern Brazil. Deep-Sea Res., 40, 293-310.

Joyce, T.M., B.A. Warren, and L. Talley, 1986: The geothermal heating of the abyssal subarctic ocean. Deep-Sea Res., 33, 1003-1015.

Karl, D., and R. Lukas, 1996: The Hawaii Ocean Time-series (HOT) program: Background, rationale and field implementation. Deep-Sea Res. II, 43, 129-156.

Lee, W.H.K., and C.S. Cox, 1966: Time variation of ocean temperatures and its relation to internal waves and oceanic heat flow measurements. 71, 2101-2111.

Lukas, R, and D. Karl, 1999: Hawaii Ocean Time-series. A Decade of Interdisciplinary Oceanography. School of Ocean and Earth Science and Technology, U. Hawaii, Technical Rept. SOEST-99-05.

Lukas, R., and F. Santiago-Mandujano, 1996: Interannual Variability of Pacific Deep and Bottom Waters Observed in the Hawaii Ocean Time-series. Deep Sea Res. II, 43, 243-255.

Lukas, R., and F. Santiago-Mandujano, 2000: High frequency abyssal variations near Hawaii. J. Geophys. Res., in preparation.

Mantyla, A.W., 1975: On the potential temperature in the abyssal Pacific Ocean. J. Mar. Res., 33, 341-354.

Mantyla, A.W. and J.L. Reid, 1983: Abyssal characteristics of the World Ocean waters. Deep-Sea Res., 30, 805-833

McCarthy M. C., L. D. Talley, and M. O. Baringer, 1997: Deep upwelling and diffusivity in the southern Central Indian Basin, Geophys. Res. Lett., 24, 2801-2804.

Mitchum, G. T., 1996: On using satellite altimetric heights to provide a spatial context for the Hawaii Ocean Time-series measurements. Deep-Sea Res. II, 43, 257-280.

Munk, W., 1966: Abyssal recipes. Deep-Sea Res., 13, 707-730.

Polzin K. L., K. G. Speer, J. M. Toole, and R. W Schmitt, 1996: Intense mixing of Antarctic Bottom Water in the equatorial Atlantic Ocean. Nature, 380, 54-57.

Polzin K. L., J. M. Toole, J. R. Ledwell, and R. W. Schmitt, 1997: Spatial variability of turbulent mixing in the abyssal ocean. Science, 276, 93-96.

Press, W. H., S. A. Teukolsky, W. T. Vetterling and B. P. Flannery, 1992: Numerical Recipes. Cambridge University Press, 963 pp.

Reid, J.L., 1969: Preliminary results of measurements of deep currents in the Pacific Ocean. Nature, 221, 848.

Reid, J.L. and P.F. Lonsdale, 1974: On the flow of water through the Samoan Passage. J. Phys. Oceanogr., 4, 58-73.

Roemmich, D., S. Hautala, and D. Rudnick, 1996: Northward abyssal transport through the Samoan passage and adjacent regions. J. Geophys. Res., 101, 14,039-14,055

Santiago-Mandujano, F., L. Tupas, C. Nosse, D. Hebel, L. Fujieki, R. Lukas and D. Karl, 1999: Hawaii Ocean Time-series Data Report 10, 1998. In: Lukas, R., and D. Karl, 1999: Hawaii Ocean Time-series. A Decade of Interdisciplinary Oceanography. School of Ocean and Earth Science and Technology, U. Hawaii, Technical Rept. SOEST-99-05.

Schwartzlose, R.A. and J.D. Isaacs, 1969: Transient circulation event near the deep ocean floor. Science, 165, 889-891.

Smith, W.H.F., and D.T. Sandwell, 1997: Global Sea Floor Topography from Satellite Altimetry and Ship Depth Soundings, Science, 277, 1956-1962.

Toole, J. M., K.L. Polzin and R. W. Schmitt, 1994: Estimates of Diapycnal Mixing in the Abyssal Ocean, Science, 264, 1120-1123.

Whitehead, J.A., 1989: Surges of Antarctic Bottom Water into the North Atlantic. J. Phys. Oceanogr., 19, 853-861.

Winn, C., R. Lukas, D. Karl, and E. Firing, 1993: Hawaii Ocean Time-series Data Report 3, 1991. School of Ocean and Earth Science and Technology, U. Hawaii, Rept. SOEST-93-3.

Wyrtki, K., L. Magaard, and J. Hager, 1976: Eddy energy in the oceans. J. Geophys. Res., 81, 2641-2646.

Table 1: Accuracy, precision and observed abyssal standard deviation for temperature, salinity, and dissolved oxygen for HOT CTD profiles. Observed standard deviation includes all HOT observations between 4700 and 4800 m.

Variable	Precision	Accuracy	Standard Deviation (below 4700 m)
Temperature (°C)	0.0002	0.0014	0.0075
Salinity	0.001	0.003	0.0015
Oxygen (μmol kg^{-1})	0.35	3	2.14

Table 2: Summary of parameters relevant to the cold events. The differences in column 4 are with respect to the median shown in Fig. 3a. Column 5 indicates the depth (or depth range) of the layer with the lowest θ.The recovery time is the e-folding time scale of the exponential fits shown in Figs. 4 and 6 (preliminary data through April, 2000 were used for Event 6.)

Cold Event	Cruise with lowest θ (month/year)	Lowest θ (°C)	Difference from median (°C)	Depth range (m)	Recovery time (days)
1	HOT-27 (6/1991)	1.086	-0.012	4695	123
2	HOT-51 (1/1994)	1.084	-0.014	4710-4720	80
3	HOT-68 (11/1995)	1.088	-0.010	4710-4730	173
4	HOT-78 (12/1996)	1.075	-0.023	4670-4725	187
5	HOT-98 (10/1998)	1.074	-0.024	4680-4725	67
6	HOT-107 (8/1999)	1.085	-0.013	4600-4725	116

FIGURE CAPTIONS

Figure 1. Bathymetric map of the central North Pacific (a) and an expanded version for the area surrounding Oahu (b) showing the location of the HOT station, ALOHA. Contours are ocean depths in kilometers, with a contour interval of 500 m (a) and 100 m (b). Depths shallower than 4500|4400 m are in dark gray and not contoured in (a)|(b); land is black. The solid triangle and diamond in (b) indicate the location of CTD casts taken on the western slope of the Maui Deep, and near the sill between the Kauai Deep and the Maui Deep. The solid lines give the hypothesized path of Pacific Bottom Water through the Horizon passage into the Northeast Pacific (Edmond et al., 1971) and as extended by this work.

Figure 2. Time series of potential temperature (°C) versus depth below 4200 m for HOT cruises 1-109. Contours are at 0.005°C intervals. Shaded regions are colder than 1.1 °C. The symbols along the bottom axis indicate dates of CTD casts. The horizontal lines indicate the depths of the bottom (solid), and of the sill between the Kauai Deep and the Maui Deep (dashed). The irregular solid line indicates the maximum depth of CTD profiles during each cruise. During the first two years of observations, few of the CTD casts were able to reach below the sill depth. The vertical dashed lines indicate the cruises when the coldest near-bottom temperatures were observed during the cold events, the event number is indicated along the top axis.

Figure 3. Potential temperature profiles deeper than 4200 m for HOT cruises 1-109 (a). The thick line connects the median values of all casts within 2-m intervals. Also shown are the

standard deviations below 4200 m (b) and skewness from the ensemble of CTD data for 2-m bins (c), as well as the number of profiles included in each bin (d).

Figure 4. Potential temperature averaged between 4590 and 4625 m during HOT cruises 25-33. Temperatures from cruises with two deep casts were averaged. The thick line is an exponential fit to the means from cruises 26-28 and 30-33.

Figure 5. Potential temperature profiles below 4400 m for HOT cruises 46-56 (a), 63-74 (b), 74-89 (c), and 96-109 (d). Each profile is labeled by its cruise number. Note that the horizontal scale has been contracted in c), d), compared to a), b). Only one cast is included for cruises with more than one deep cast, except for cruise 98 in which the second deep cast is labeled 98'.

Figure 6. Potential temperature averaged between 4680 and 4707 m during cruises 49 through 109 (black circles). Temperatures from cruises with two deep casts were averaged, except for cruise 98 in which the second deep cast is labeled 98'. The thick line is an exponential least squares fit to the means from cruises 51 to 56, 68 to 74, 78 to 89, and 98' to 106.

Figure 7. Salinity profiles smoothed with a 14-m running mean filter for HOT cruises 74-79 (a). Dissolved oxygen profiles smoothed with a 58-m running mean filter for HOT cruises 74-81 (b).

Figure 8. Salinity (a), and dissolved oxygen (b) CTD profiles from cruise HOT-98, smoothed with 14-m and 34-m running mean filters respectively. The dashed line is the first cast of the cruise, and the solid line is a cast taken 46 hours later. The shaded area is ± one standard deviation from the median (dotted line) from cruises 1 through 109.

Figure 9. Bottom depth following the path indicated in Fig. 1a (a). The area between the vertical dashed lines is expanded in (b), showing the Maui Deep, the Kauai Deep and the sill that separates these two basins. The drawing in (b) represents the flow of cold and salty water cascading over the sill with a transport *Tr*, filling the Kauai Deep from the bottom with an upwelling speed *w*.

Figure 10. Potential temperature (a), and salinity (b) plotted against depth below 4200 m from profiles at station ALOHA (HOT-92), on the western slope of the Maui Deep, and near the sill separating the Maui Deep from the Kauai Deep. See Fig. 1b for the location of these stations. Potential temperature plotted against salinity for these profiles (c), with isolines of constant σ_5 dashed (scale on right axis). The salinity profiles were smoothed with a 14-dbar running mean filter.

Figure 11. Area and volume enclosed by isobaths in the Kauai Deep as a function of depth, calculated from ETOPO5 bathymetry data. Upwelling speed as a function of depth for a constant overflow of 0.05 Sv into the basin, along with the duration of the overflow required for the water to reach a specified level in the Kauai Deep. The horizontal dashed line indicates the bottom of station ALOHA.

Figure 12. Illustration of hypothetical seiching in the Kauai Deep. Each panel represents the Kauai Deep at different phases of the seiche. The parallel lines are isotherms, where thicker lines indicate colder temperatures, and the vertical line indicates the location of the HOT site. In a) the seiching causes a sinking of the warm isotherms at the HOT site and a lifting of the cold water on the opposite side of the basin. In b) the isotherms are undisturbed, and in c) the cold isotherms move upwards at the HOT site.

Figure 13. Heat content from mid-1993 through 1999 in the Kauai Deep between 4488 and 4685 m calculated from CTD profiles and bathymetry data (equation (2) in the text). The arrowheads along the bottom axis indicate times of CTD casts. The vertical dashed lines indicate the cruises when the coldest near-bottom temperatures were observed during the last five cold events.

Figure 14. Mean potential temperature between 4620 and 4670 m from HOT cruises, after removing the median from cruises 1 to 109 (top plot, scale on the left axis), and potential temperature averaged between 4610 and 4620 m during cruises HOT-1-109 (second plot from the top, scale on the right axis). Temperatures from cruises with two deep casts were averaged. Dynamic height from inverted echo sounders after the removal of the semi-diurnal and diurnal tides and variability with time scales less than a day (middle plot, scale on the left axis). The record at station ALOHA is labeled, and the record above it is located near Kaena Pt. (21° 50.8'N, 158° 21.8'W), this record is offset 0.2 dyn-m with respect to the record at ALOHA. The dotted line is an average from three other IESs located 10-20 km east, southwest and southeast of the HOT site. All records have been calibrated by CTD casts. TOPEX/Poseidon altimeter data at the HOT site (second plot from the bottom, scale on the right axis). Hawaiian boundary barotropic meridional transport (bottom plot, scale on the left axis, positive is northward), from Firing et al. (1999). The vertical dashed lines indicate the cruises when the coldest near-bottom temperatures were observed during the six cold events. The labels on the top axis indicate the event number.

Figure 15. Time-longitude contours of the interannual sea-level signal at the latitude of the HOT site from the TOPEX/Poseidon altimeter data, after eliminating the annual harmonic obtained by direct least squares fitting, and suppressing the intra-annual signal by low-pass filtering the residuals with a 130-day running mean (Mitchum, 1996). Regions with negative anomalies are shaded and the contour interval is 4 cm. The vertical line indicates the location of the HOT site. The horizontal lines indicate the cruises when the coldest near-bottom temperatures were observed during cold events two through five.

Figure 16. Model simulation of the third event overflow as discussed in the text, with a transport of 0.18 Sv across the sill, and with a constant diffusivity of 7×10^{-4} $m^2 s^{-1}$. The warmest curve is the initial condition profile, and the following curves are temperature distributions at 10-day intervals. The coldest curve (thick line) is after 110 days.

Figure 17. Vertical and temporal variability of the vertical eddy diffusivity (K_v) during the relaxation phase of the cold events obtained from Equation (6) as discussed in the text. Median values of K_v between 4000 m and near the bottom during the 2^{nd}, 3^{rd}, 5^{th} and 6^{th} cold events (a). Depth versus time contours of K_v during the relaxation phase of the second event (b). The horizontal line indicates the depth of the sill between the Kauai Deep and the Maui Deep. The arrowheads along the bottom axis in (b) indicate times of CTD casts.

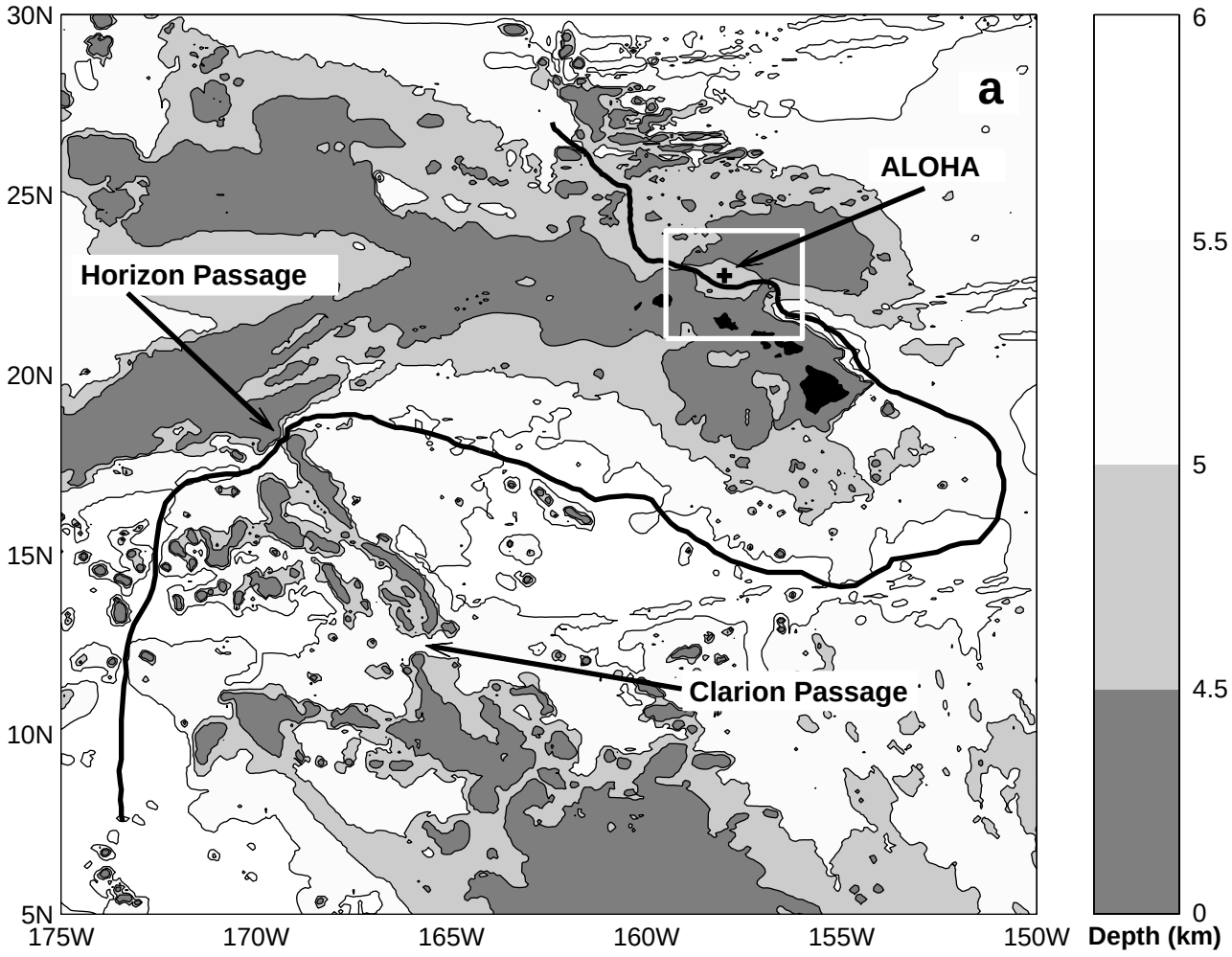
30N
25N
20N
15N
10N
5N
175W
170W
165W
160W
155W
150W
a
ALOHA
Horizon Passage
Clarion Passage
6
5.5
5
4.5
0
Depth (km)

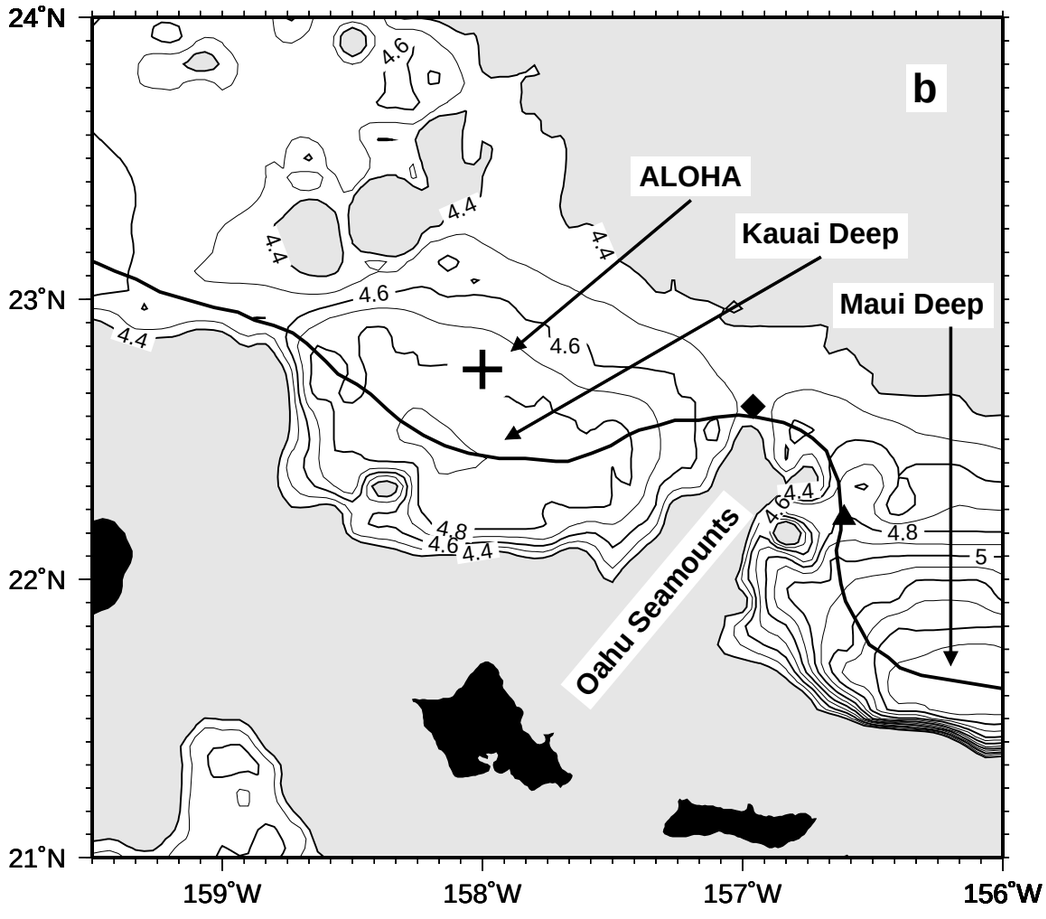
24°N
23°N
22°N
21°N
159°W
158°W
157°W
156°W
b
ALOHA
Kauai Deep
Maui Deep
Oahu Seamounts
4.4
4.6
4.8
5

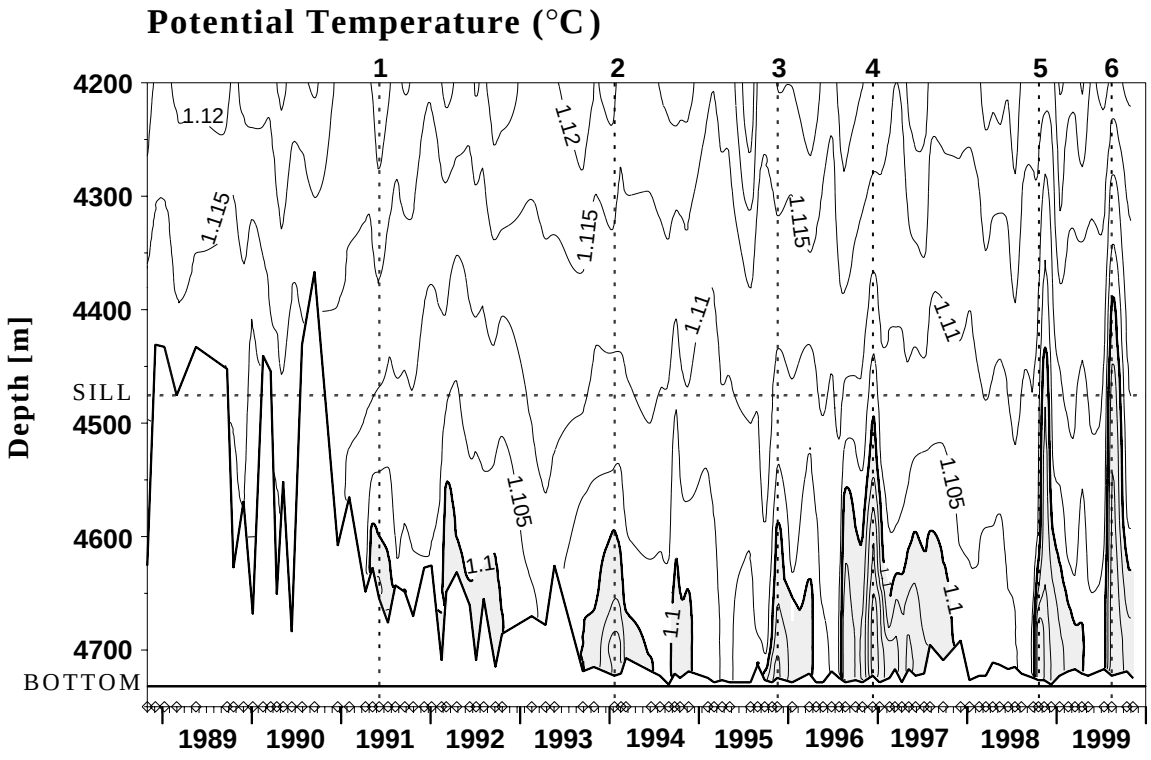
Potential Temperature (°C)
Depth [m]
4200
4300
4400
4500
4600
4700
SILL
BOTTOM
1
2
3
4
5
6
1.12
1.115
1.11
1.105
1.1
1989
1990
1991
1992
1993
1994
1995
1996
1997
1998
1999

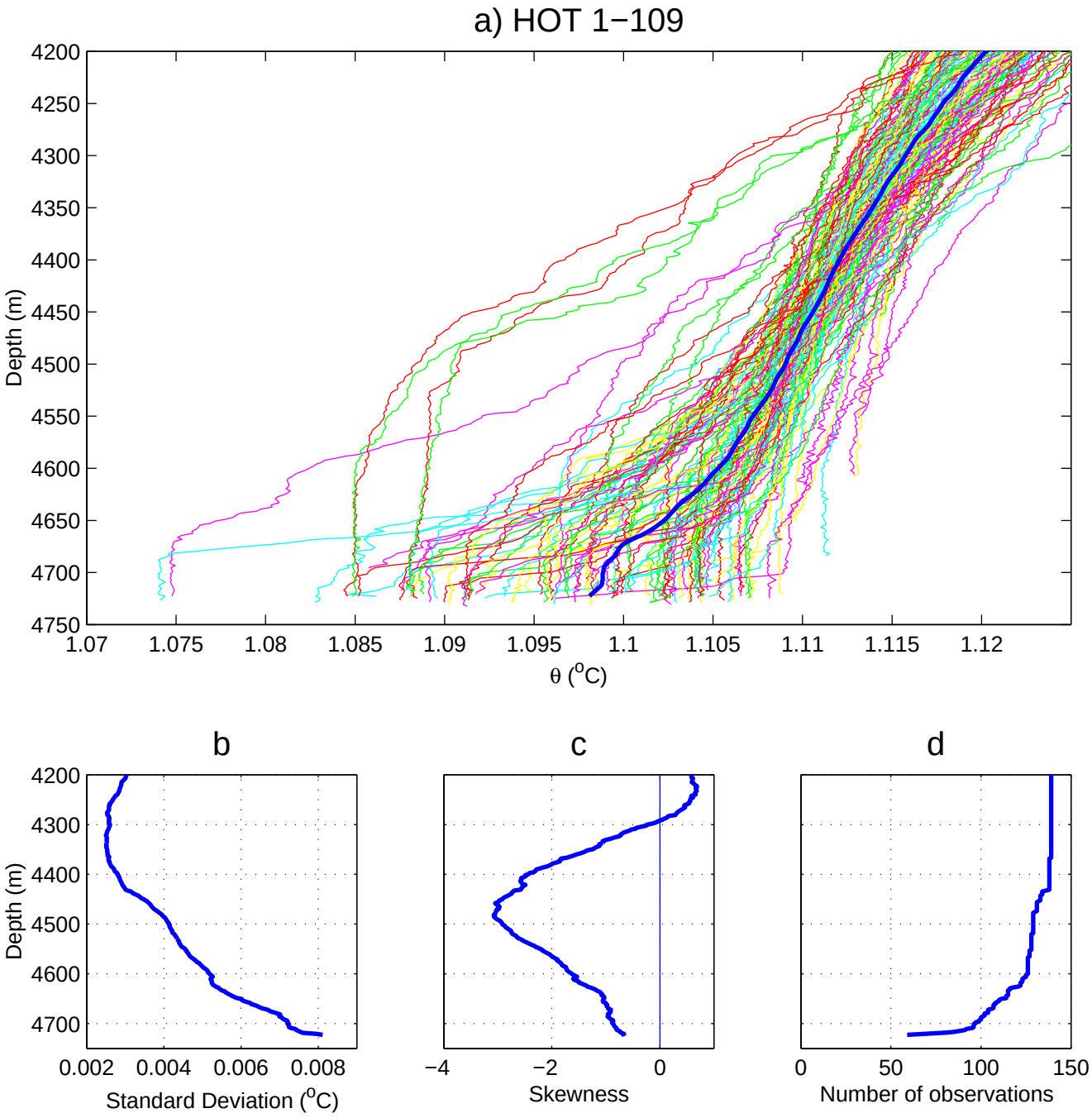
a) HOT 1−109
Depth (m)
θ (°C)
b
c
d
Standard Deviation (°C)
Skewness
Number of observations

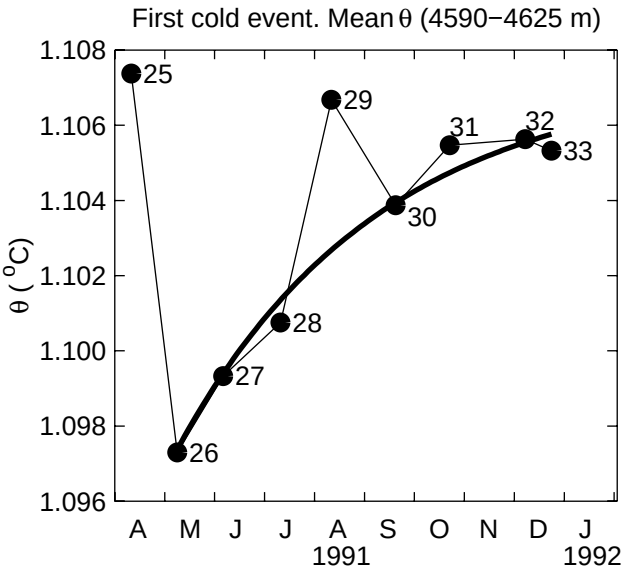
First cold event. Mean θ (4590−4625 m)
θ (°C)
1.108
1.106
1.104
1.102
1.100
1.098
1.096
25
26
27
28
29
30
31
32
33
A
M
J
J
A
S
O
N
D
J
1991
1992

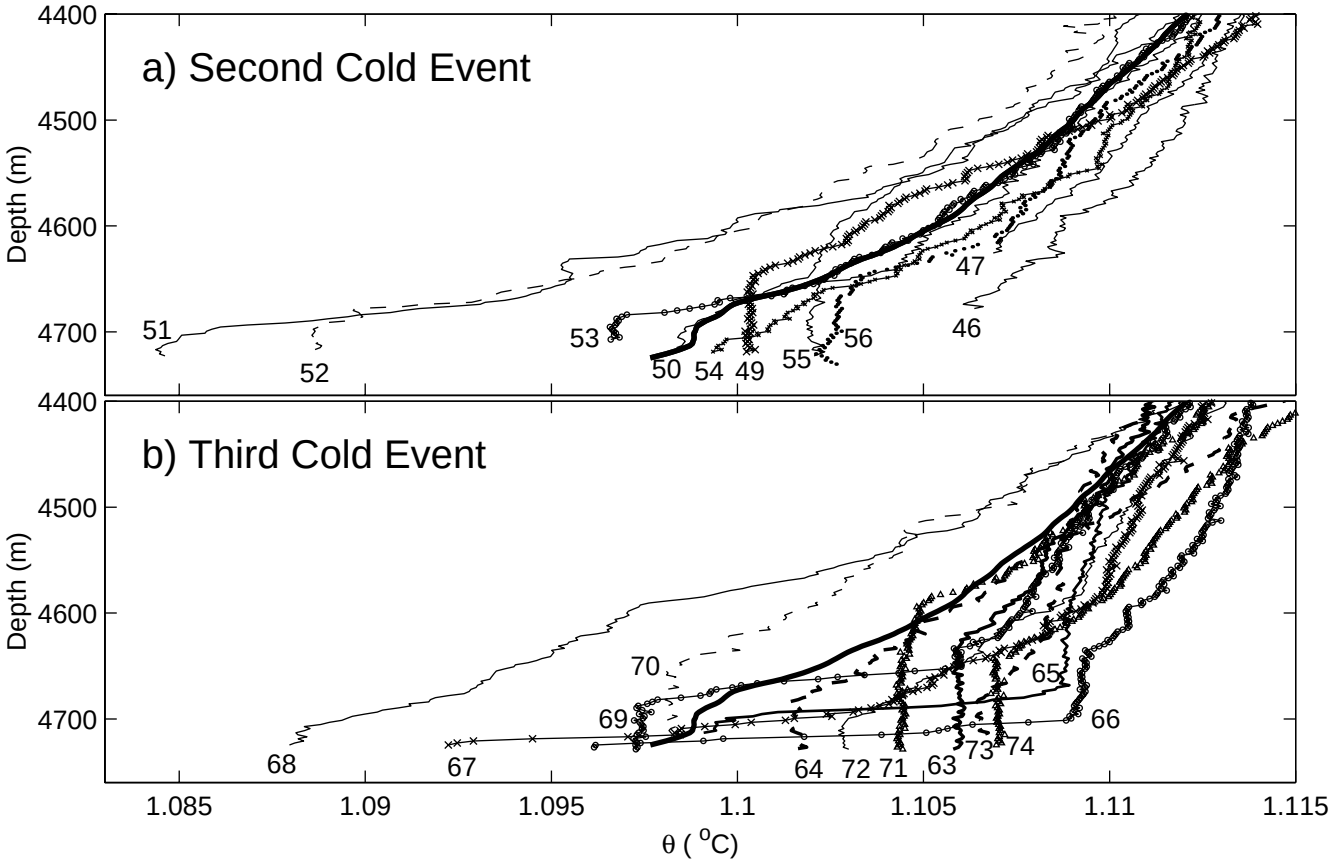
a) Second Cold Event
Depth (m)
4400
4500
4600
4700
51
52
53
50
54
49
55
56
47
46

b) Third Cold Event
Depth (m)
4400
4500
4600
4700
70
65
69
66
68
67
64
72
71
63
73
74
1.085
1.09
1.095
1.1
1.105
1.11
1.115
θ (°C)

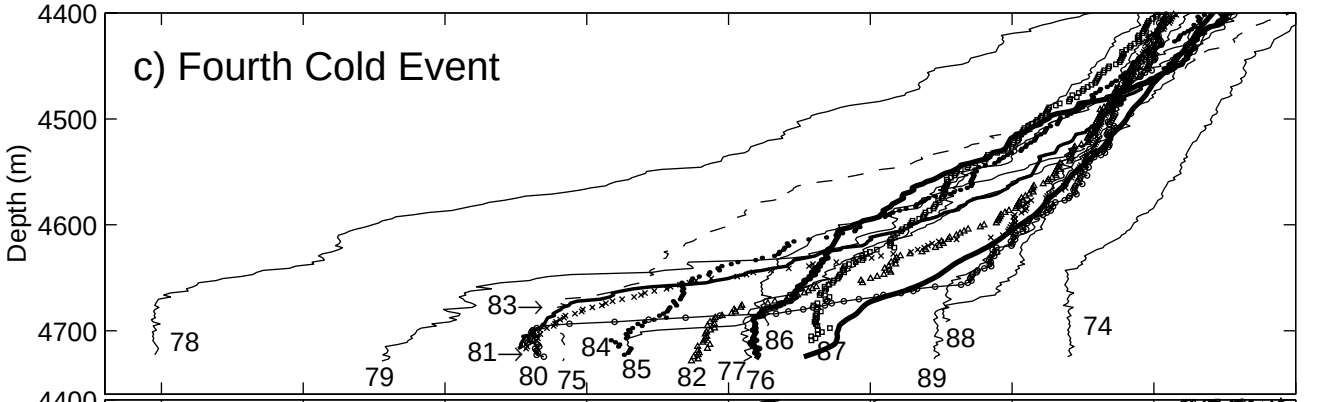
c) Fourth Cold Event
Depth (m)
4400
4500
4600
4700
78
83
81
79
80
75
84
85
82
77
86
76
87
88
74
89

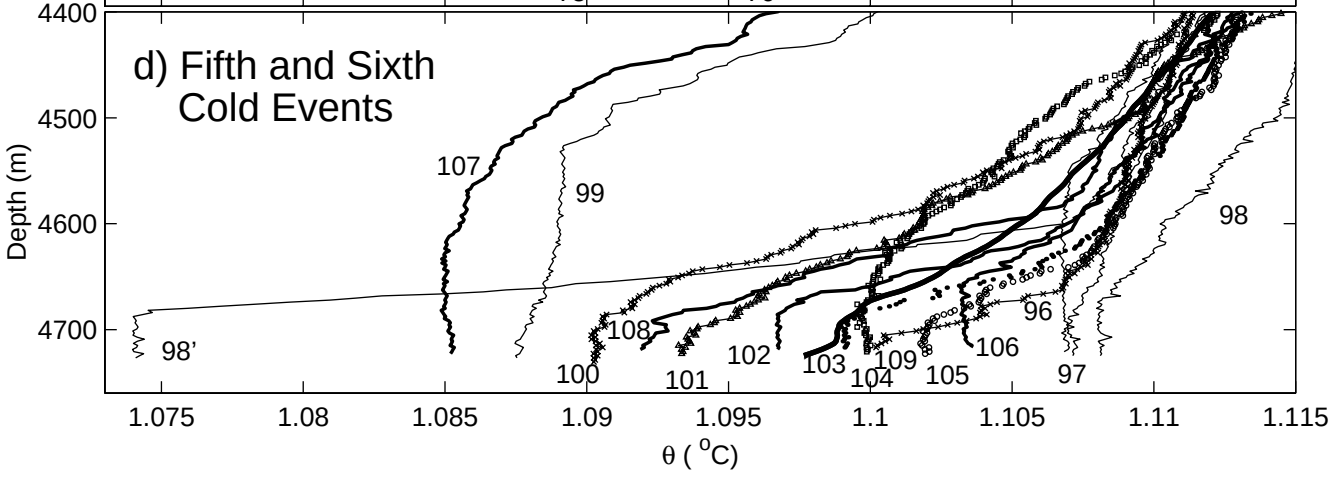
d) Fifth and Sixth
Cold Events
Depth (m)
4400
4500
4600
4700
107
99
98
98'
108
96
100
101
102
103
104
109
105
106
97
1.075
1.08
1.085
1.09
1.095
1.1
1.105
1.11
1.115
θ (°C)

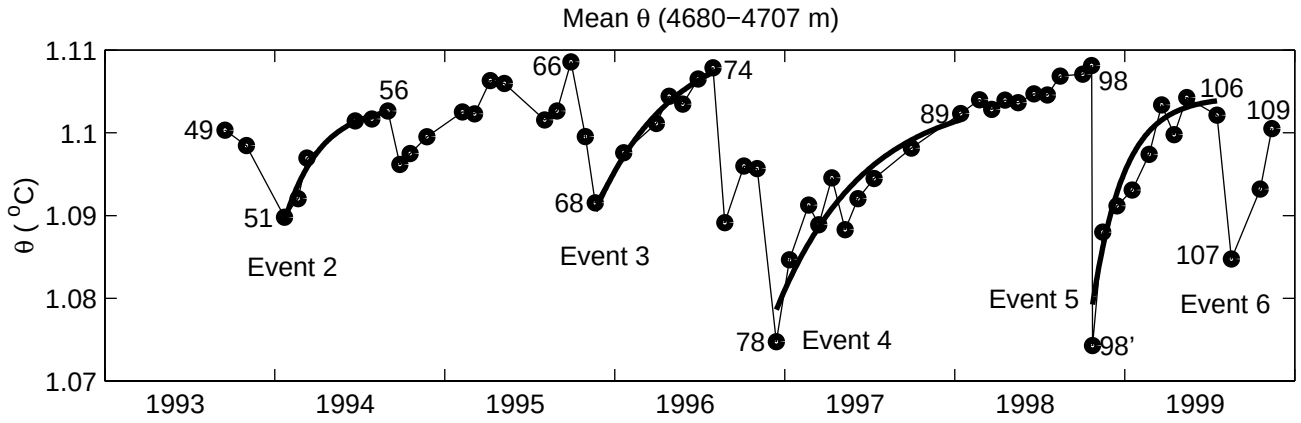
Mean θ (4680−4707 m)
θ (°C)
1.11
1.1
1.09
1.08
1.07
1993
1994
1995
1996
1997
1998
1999
49
51
56
66
68
74
78
89
98
98'
106
107
109
Event 2
Event 3
Event 4
Event 5
Event 6

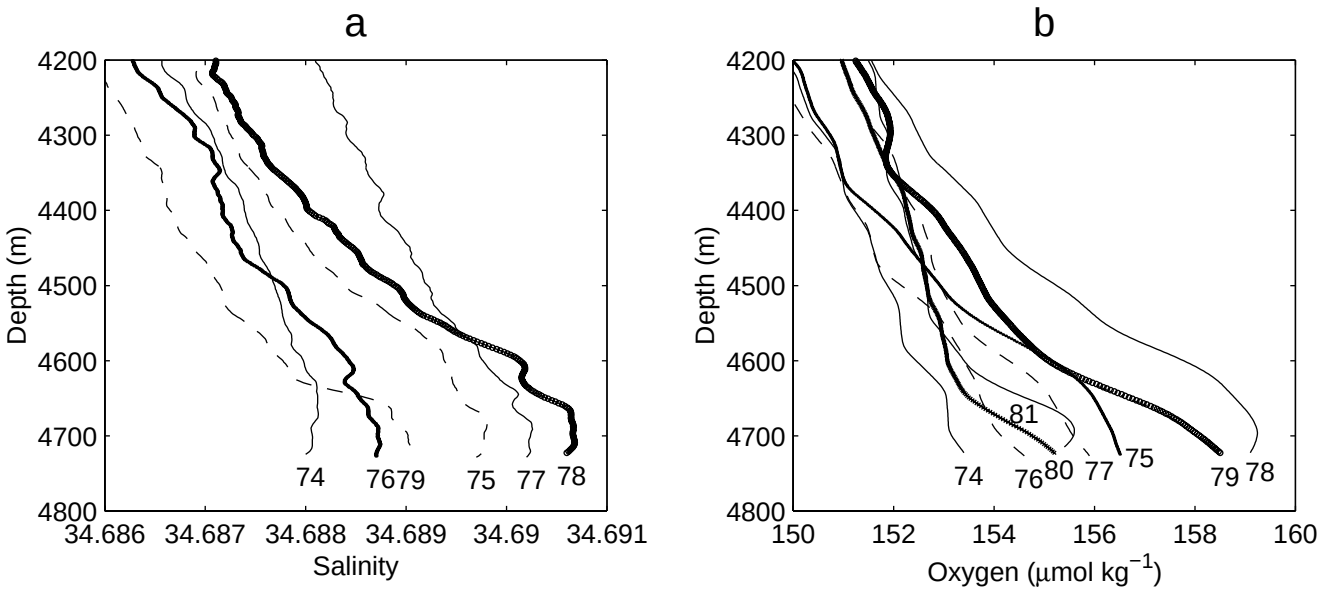
a
b
Depth (m)
4200
4300
4400
4500
4600
4700
4800
34.686
34.687
34.688
34.689
34.69
34.691
Salinity
74
76
79
75
77
78
150
152
154
156
158
160
Oxygen (µmol kg^{-1})
81
80

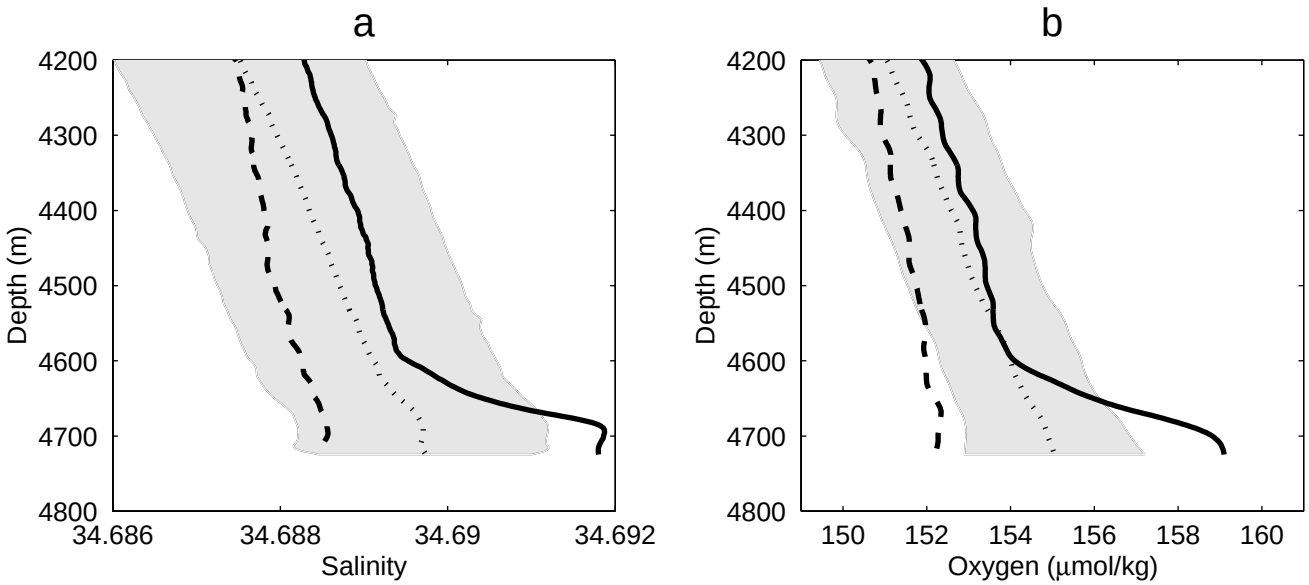
a
b
4200
4300
4400
4500
4600
4700
4800
Depth (m)
34.686
34.688
34.69
34.692
Salinity
150
152
154
156
158
160
Oxygen (µmol/kg)

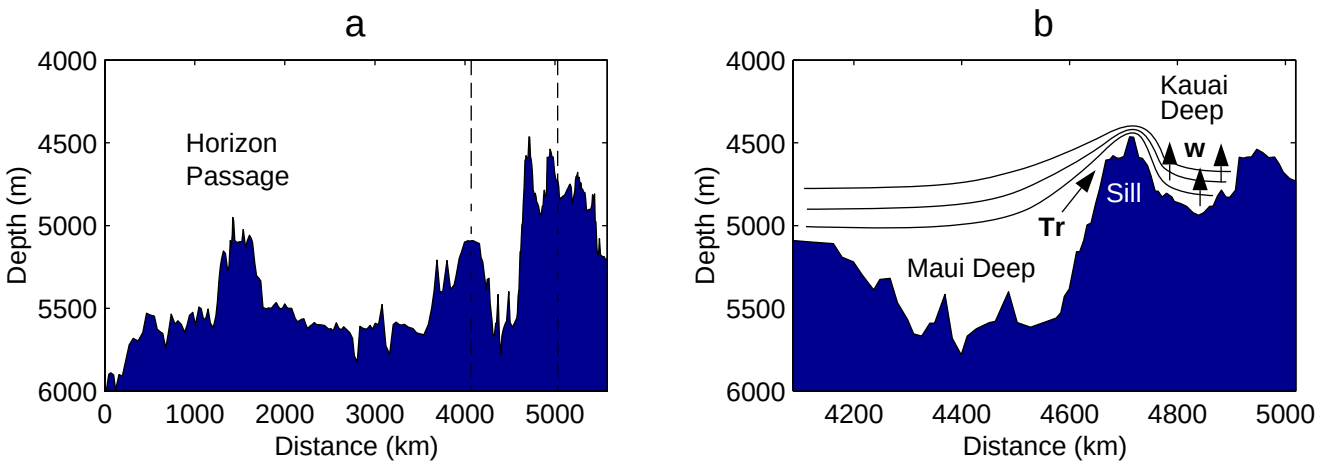
a
b
Horizon
Passage
Depth (m)
Distance (km)
Kauai
Deep
w
Sill
Tr
Maui Deep

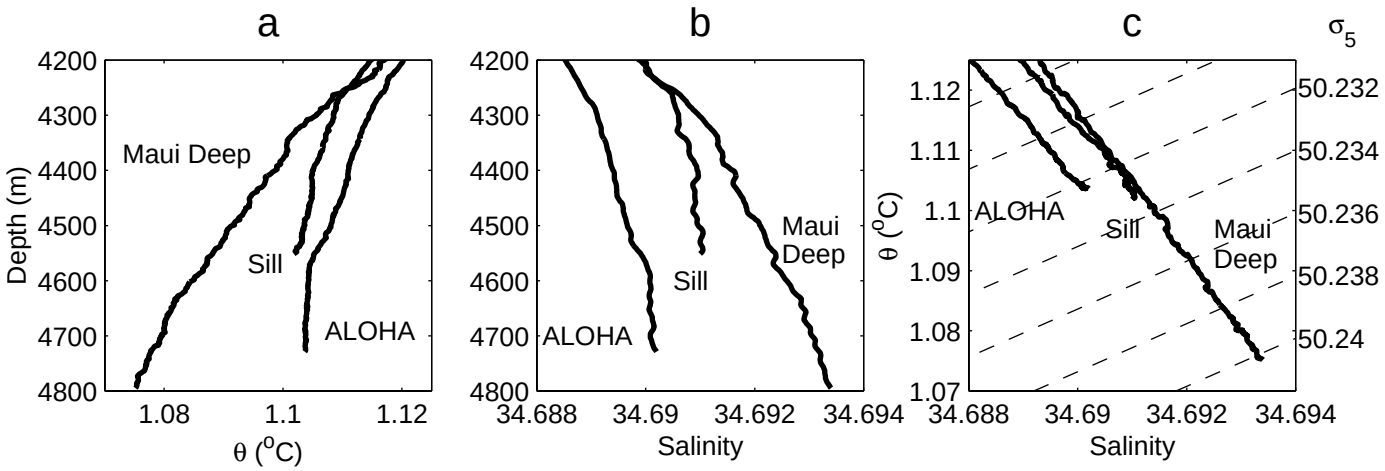
a
b
c
σ_5
Depth (m)
4200
4300
4400
4500
4600
4700
4800
Maui Deep
Sill
ALOHA
1.08
1.1
1.12
θ (°C)
34.688
34.69
34.692
34.694
Salinity
Maui
Deep
Sill
ALOHA
θ (°C)
1.12
1.11
1.1
1.09
1.08
1.07
ALOHA
Sill
Maui
Deep
50.232
50.234
50.236
50.238
50.24
Salinity

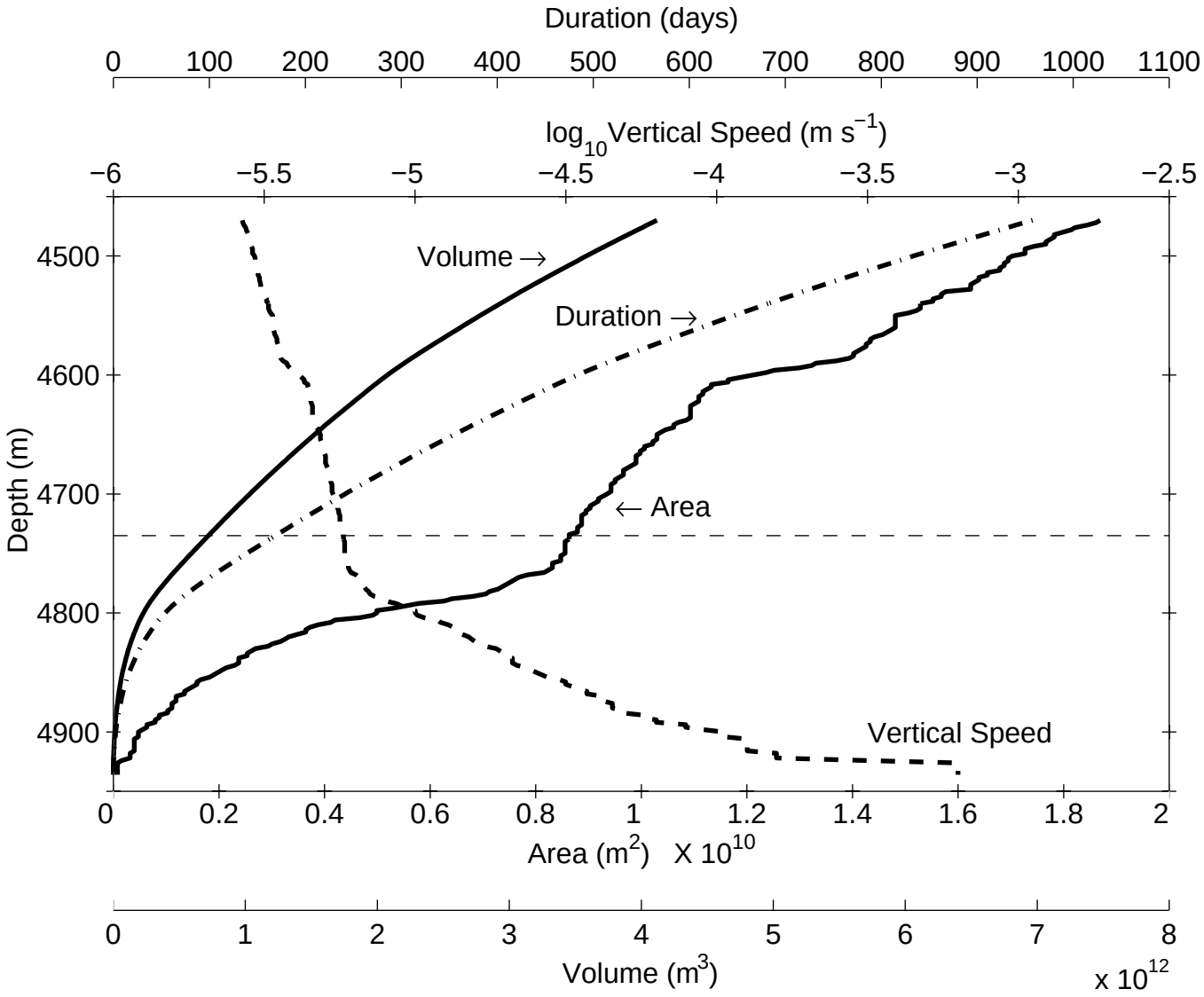
Duration (days)
0
100
200
300
400
500
600
700
800
900
1000
1100
log10Vertical Speed (m s−1)
−6
−5.5
−5
−4.5
−4
−3.5
−3
−2.5
Volume →
Duration →
← Area
Vertical Speed
Depth (m)
4500
4600
4700
4800
4900
0
0.2
0.4
0.6
0.8
1
1.2
1.4
1.6
1.8
2
Area (m2) X 10^10
0
1
2
3
4
5
6
7
8
Volume (m3)
x 10^12

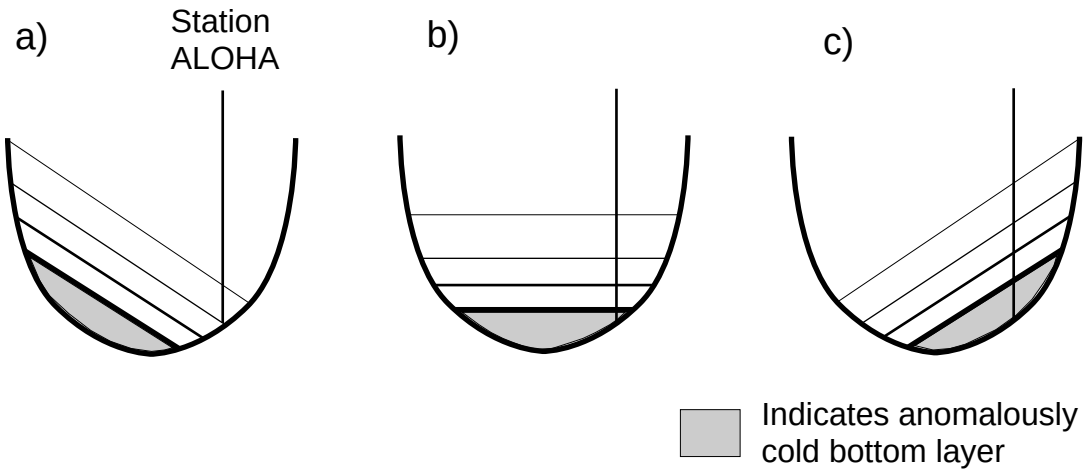
a)
Station
ALOHA
b)
c)
Indicates anomalously
cold bottom layer

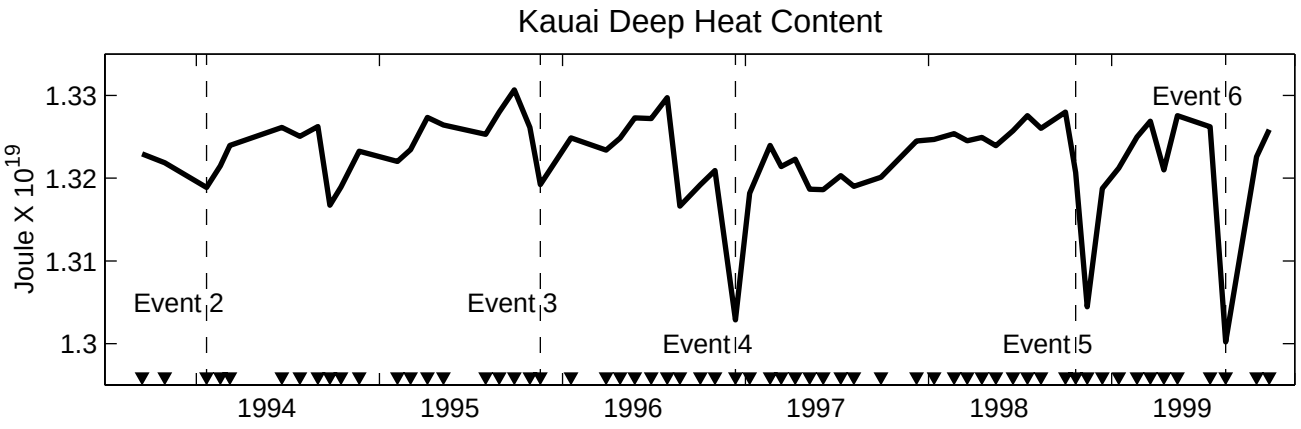
Kauai Deep Heat Content
Joule X 10^19
1.33
1.32
1.31
1.3
Event 2
Event 3
Event 4
Event 5
Event 6
1994
1995
1996
1997
1998
1999

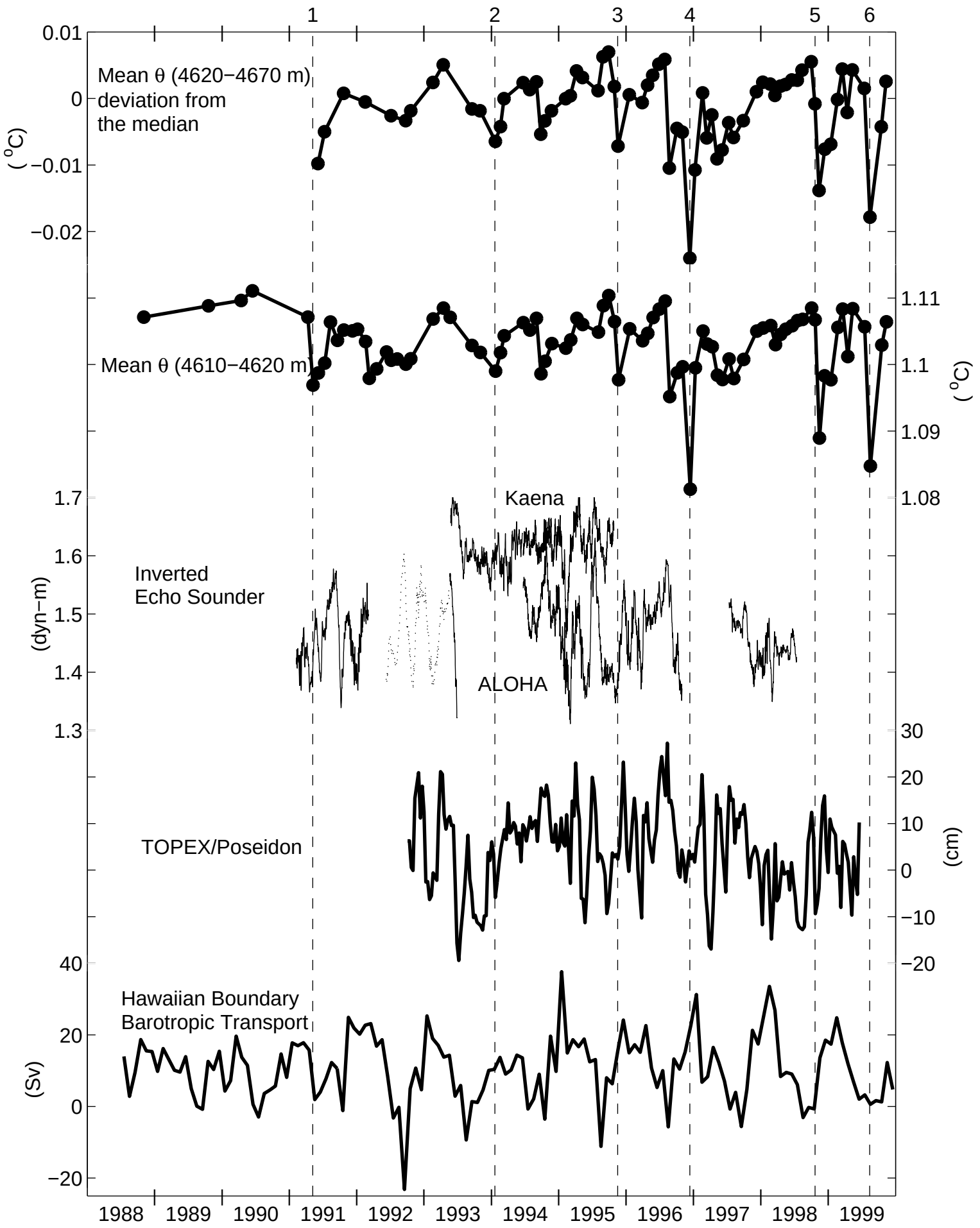
1
2
3
4
5
6
0.01
0
−0.01
−0.02
(°C)
Mean θ (4620−4670 m)
deviation from
the median
Mean θ (4610−4620 m)
1.11
1.1
1.09
1.08
(°C)
1.7
1.6
1.5
1.4
1.3
(dyn−m)
Kaena
Inverted
Echo Sounder
ALOHA
30
20
10
0
−10
−20
(cm)
TOPEX/Poseidon
40
20
0
−20
(Sv)
Hawaiian Boundary
Barotropic Transport
1988
1989
1990
1991
1992
1993
1994
1995
1996
1997
1998
1999

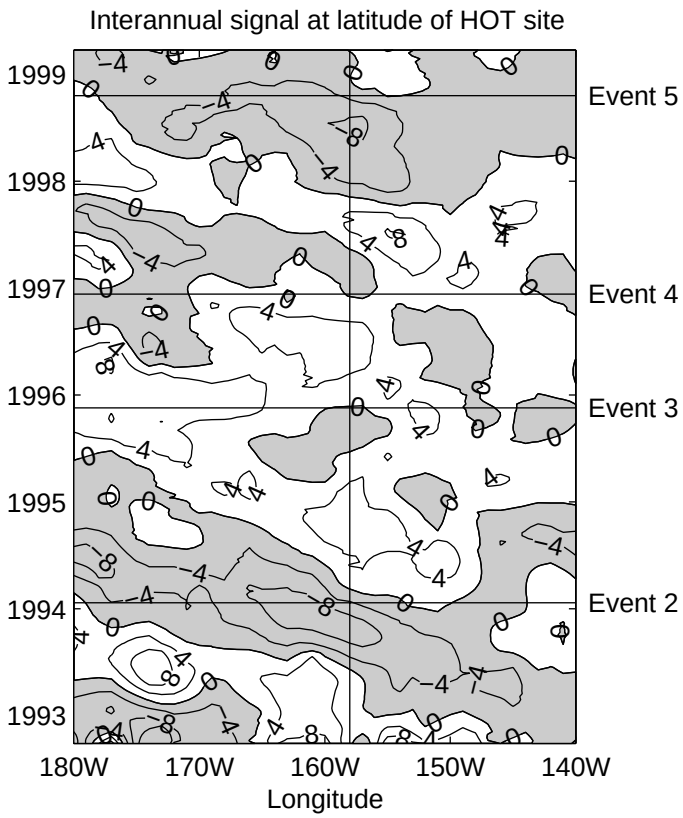
Interannual signal at latitude of HOT site
1999
1998
1997
1996
1995
1994
1993
Event 5
Event 4
Event 3
Event 2
180W
170W
160W
150W
140W
Longitude

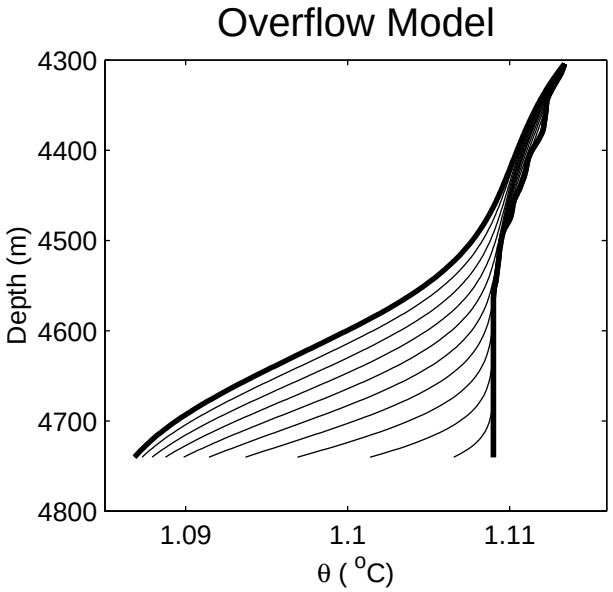
Overflow Model
4300
4400
4500
4600
4700
4800
Depth (m)
1.09
1.1
1.11
θ (°C)

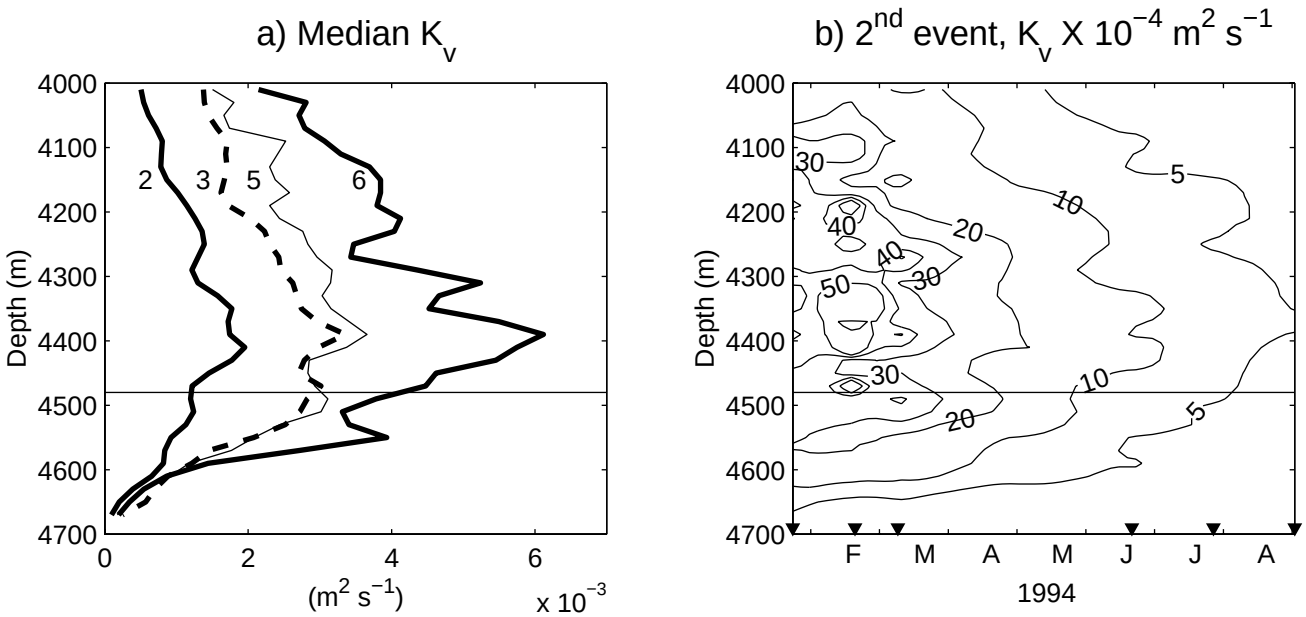
a) Median K_v
b) 2nd event, K_v X 10^{-4} m^2 s^{-1}
Depth (m)
4000
4100
4200
4300
4400
4500
4600
4700
2
3
5
6
0
2
4
6
(m^2 s^{-1})
x 10^{-3}
30
40
50
20
10
5
F
M
A
M
J
J
A
1994